The EMBO Journal (2011) 30, 3895–3912 | © 2011 European Molecular Biology Organization | All Rights Reserved 0261-4189/11
www.embojournal.org

THE EMBO JOURNAL

Calcium microdomains at the immunological synapse: how ORAI channels, mitochondria and calcium pumps generate local calcium signals for efficient T-cell activation

Ariel Quintana[1,7,*], Mathias Pasche[2,6,7], Christian Junker[1,7], Dalia Al-Ansary[1], Heiko Rieger[3], Carsten Kummerow[1], Lucia Nuñez[4], Carlos Villalobos[4], Paul Meraner[5], Ute Becherer[2], Jens Rettig[2], Barbara A Niemeyer[1] and Markus Hoth[1,*]

[1]Department of Biophysics, Saarland University, Homburg, Germany, [2]Department of Physiology, Saarland University, Homburg, Germany, [3]Department of Theoretical Physics, Saarland University, Saarbrücken, Germany, [4]Institute of Biology and Molecular Genetics, University of Valladolid and CSIC, Valladolid, Spain and [5]Signaling and Gene Expression Research, Department of Pathology, La Jolla Institute for Allergy and Immunology, La Jolla, CA, USA

Cell polarization enables restriction of signalling into microdomains. Polarization of lymphocytes following formation of a mature immunological synapse (IS) is essential for calcium-dependent T-cell activation. Here, we analyse calcium microdomains at the IS with total internal reflection fluorescence microscopy. We find that the subplasmalemmal calcium signal following IS formation is sufficiently low to prevent calcium-dependent inactivation of ORAI channels. This is achieved by localizing mitochondria close to ORAI channels. Furthermore, we find that plasma membrane calcium ATPases (PMCAs) are re-distributed into areas beneath mitochondria, which prevented PMCA up-modulation and decreased calcium export locally. This nano-scale distribution—only induced following IS formation—maximizes the efficiency of calcium influx through ORAI channels while it decreases calcium clearance by PMCA, resulting in a more sustained NFAT activity and subsequent activation of T cells.

The EMBO Journal (2011) **30,** 3895–3912. doi:10.1038/emboj.2011.289; Published online 16 August 2011
Subject Categories: membranes & transport; immunology
Keywords: calcium signals; immunological synapse; mitochondria; ORAI channels; PMCA

*Corresponding authors. A Quintana, La Jolla Institute for Allergy and Immunology, La Jolla, CA 92037, USA and Department of Pathology, Immune Disease Institute, Harvard University, 200 Longwood Avenue, Room 152, Boston, MA 02115, USA. Tel.: +1 857 919 2822; Fax: +1 858 752 6984; E-mail: quintana@liai.org or quintana@idi.harvard.edu or M Hoth, Medical Faculty, Saarland University, Building 58, D-66421, Homburg, Germany. Tel.: +49 6841 1626266 (1626267); Fax: +49 6841 1626060; E-mail: markus.hoth@uks.eu
[6]Present address: MRC Laboratory of Molecular Biology, Hills Road, Cambridge, UK
[7]These authors contributed equally to this work

Received: 19 November 2010; accepted: 19 July 2011; published online: 16 August 2011

Introduction

T-helper (T_h) cells are activated through formation of a stable junction with antigen-presenting cells, the immunological synapse (IS). The formation of an IS secures efficient activation of T-cell receptors (TCR) by overcoming several obstacles that hinder their unwanted activation, including the low affinity of TCR for its ligand, the low number of specific ligands available to activate a particular TCR, the small dimensions of TCR and the random localization of cytosolic signalling proteins (Dustin, 2008).

A crucial step for the successful activation of T_h cells following TCR ligand binding is the stimulation of calcium (Ca^{2+}) entry across the plasma membrane (PM) through the gating of Ca^{2+} release-activated Ca^{2+} (CRAC) channels, encoded by the ORAI proteins, which constitute the major Ca^{2+} influx pathway in T cells (Feske *et al*, 2005; Feske, 2007). However, an increase in the intracellular Ca^{2+} concentration ($[Ca^{2+}]_i$) activates a plethora of responses within cells, including secretion, motility, growth and differentiation (Feske, 2007; Oh-hora and Rao, 2008). Therefore, one of the main challenges to optimize the information capacity of a Ca^{2+} signal is to maintain its signalling specificity. Besides amplitude and kinetics, local Ca^{2+} signals or Ca^{2+} microdomains can generate specificity. It has been reported that Ca^{2+} microdomains regulate neuronal function (Roberts, 1993; Prakriya *et al*, 1996), neurotransmitter release (Llinas *et al*, 1992a, b), neuronal growth (Spitzer, 2006), mast cell activation (Kar *et al*, 2011), muscle contraction and gene expression (Cannell *et al*, 1995; Dolmetsch *et al*, 2001). In all of these examples, close positioning of Ca^{2+} channels to their targets guarantees the robustness, speed and selectivity of the effectors. However, the generation of local Ca^{2+} microdomains beneath ORAI channels and their local effect on other Ca^{2+} targets at the IS still remains elusive. This study was designed to measure Ca^{2+} microdomains generated by ORAI channels at the IS, and to analyse their effect on T_h-cell function.

Results

ORAI channel, PMCA and mitochondria localization relative to the IS

Formation of a mature IS induces cell polarization, which involves the re-distribution of PM and cytosolic signalling proteins, re-organization of actin cytoskeleton and organelle re-localization (Sanchez-Madrid and del Pozo, 1999; Dustin and Cooper, 2000). The localization of ORAI channels in the PM is a crucial factor for local Ca^{2+} influx in T cells. Two recent studies have analysed ORAI1 and its activator STIM1 localization following IS formation. Lioudyno *et al* (2008) showed that ORAI1 was accumulated at the IS, and Barr *et al*

(2008) observed the localization of ORAI1 in puncta and dynamic caps everywhere in the PM, often within the vicinity of the IS, but also at the distal pole (DP). We repeated the ORAI1 localization analysis following IS formation between T cells and Raji cells pulsed with *Staphylococcus aureus* enterotoxin E (SEE). IS formation was confirmed by actin accumulation at the IS in a ring-like structure (Supplementary Figure S1A; Supplementary Movie S1) and by CD3 accumulation (best seen in Supplementary Figure S1B, cut view), which was always observed at contact sites between T cells and SEE-pulsed Raji cells ($n = 203$ T-cell Raji cell contacts). We analysed endogenous ORAI1 protein localization in Jurkat T cells, in a stable Jurkat T-cell line with relatively low amounts of HA-tagged ORAI1 and in Jurkat T cells transiently overexpressing ORAI1–mEGFP and STIM1–TagRFP-T. We found that STIM1 co-accumulated with ORAI1 at the DP at early time points and both signals moved to the IS over time (Figure 1A; Supplementary

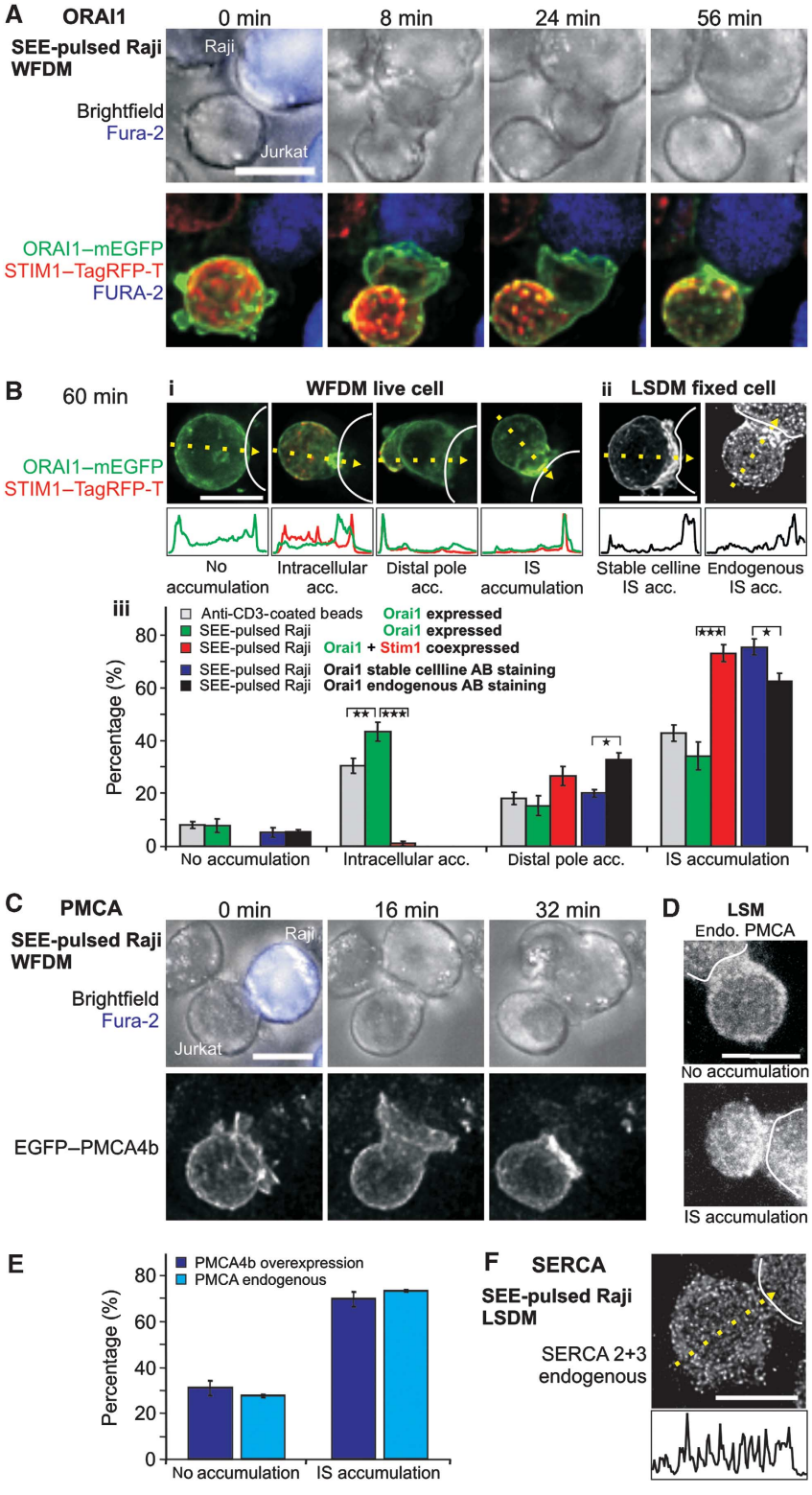

Movie S2). To quantify the ORAI1 localization, we analysed and scored the cells as shown in Figure 1B. Multiple transfections were performed, which allowed a statistical analysis of the categorical quantification. Enrichment at the IS was observed already 8 min after contact (Figure 1A) and quantified after 60 min to be present in 72% of the cells transiently overexpressing STIM1 and ORAI1 ($n = 109$ T-cell Raji cell contacts; Figure 1B, red bars). STIM1 was co-accumulating at the IS in 98% of these cases (data not shown). In 27% of the cells, a slight accumulation of ORAI1 at distal sites was observed. A similar distribution of ORAI1 was found in the stable cell line and also after immune fluorescence of endogenous ORAI1 with an anti-ORAI1 antibody (Figure 1B). Antibody specificity was confirmed by both western blots and immune-chemistry using ORAI1 siRNA and nsRNA (data not shown). ORAI1 downregulation following siRNA transfection was confirmed by qRT–PCR and western blot (data not shown).

ORAI1 accumulation at the IS was also observed when STIM1 was not co-overexpressed (Supplementary Figure S1A; Supplementary Movies S1 and S3). In this case, however, in ~40% of the cells, ORAI1 was localized to a compartment, which was clearly not part of the PM but enriched at the IS (see Supplementary Figure S1B and Figure 1B for statistics). Most likely, this intracellular compartment is part of the Golgi apparatus, which is also re-localized towards the IS (Kupfer *et al*, 1983; Kupfer and Singer, 1989). About 50% of all Orai1–mEGFP (without concomitant STIM1 overexpression) cells showed this intracellular structure. Exclusive accumulation of this structure at the IS was usually only observed without STIM1 co-expression (Figure 1B). ORAI1 was also present at the contact site between anti-CD3 antibody-coated beads and T cells (Supplementary Figure S1C) and enriched in a percentage of cells similar to SEE-pulsed Raji T-cell contacts (Figure 1B). Actin re-localization at the bead T-cell contact site confirmed a successful IS formation ($n = 234$ cells; Supplementary Figure S1D; Supplementary Movie S4).

Because the PM Ca^{2+} ATPase (PMCA) is the major Ca^{2+} extrusion pathway in T cells (Bautista *et al*, 2002), PMCA distribution is important for the shape of local Ca^{2+} signals as well. PMCA4b is the PMCA subtype highly expressed in T cells (Bautista *et al*, 2002). We analysed the localization of PMCA in Jurkat T cells expressing EGFP–PMCA4b (Figure 1C; Supplementary Movie S5) or endogenous PMCA (Figure 1D) after IS formation with SEE-pulsed Raji cells. We observed an even PM distribution, which accumulated at the IS in ~70% of the cells (Figure 1E). Finally, we analysed endogenous SERCA subtype 2 and 3 following IS formation but could not detect any preferential location with regard to the IS ($n = 117$ cells). Similar results were obtained after staining with SERCA antibodies following the induction of the IS on a coverslip coated with anti-CD3 antibodies in confocal microscopy (data not shown).

Total internal reflection fluorescence microscopy (TIRFM) has been previously used to study the localization of signalling molecules within the IS plane (Dustin and Cooper, 2000; Dustin, 2005, 2008), as it selectively reports fluorescence within about 200 nm from the PM. We analysed Jurkat T cells on anti-CD3 antibody-coated coverslips with TIRFM to measure only signals from the IS plane. All cells (47 from 3 experiments) showed the characteristic actin ring in the TIRF plane as a hallmark of successful IS formation (Figure 2A); this was not observed in uncoated control coverslips. ORAI1 was clearly located in the TIRF plane and accumulated slightly over time (Figure 2A and E) and co-localized with STIM1 (Figure 2B). Localization of PMCA at the IS was also always observed in TIRFM experiments (Figure 2C, $n = 33$ cells). Localization of ORAI1 and its enrichment at the IS was also confirmed with the stable ORAI1 cell line (Figure 2D and E). In summary, ORAI1 and PMCA4b are always present at the IS and in about 70% of the cells even enriched at the IS.

Mitochondria play an important role for the Ca^{2+} homeostasis in T cells and have been reported to accumulate at the IS in T cells (Quintana *et al*, 2007, 2009; Contento *et al*, 2010; Schwindling *et al*, 2010; Yog *et al*, 2010; Baixauli *et al*, 2011) and in natural killer cells as well (Abarca-Rojano *et al*, 2009). Mitochondrial accumulation at the IS depends on several factors including TCR activation and Ca^{2+} signalling (Quintana *et al*, 2007; Schwindling *et al*, 2010), LFA-1 activation (Contento *et al*, 2010) and the fission factor DRP-1 (Baixauli *et al*, 2011). The preferential localization of mitochondria beneath the IS was found to be essential for sustaining the activity of ORAI channels by preventing local accumulation of inflowing Ca^{2+} near the sites that govern channel inactivation (Quintana *et al*, 2007). Concomitantly, mitochondria at the IS take up more Ca^{2+} than those localized further away from the IS (Quintana *et al*, 2007, 2009).

To test the relative positioning between mitochondria, ORAI1 channels and PMCA at the IS, we performed a co-localization analysis using TIRFM (Figure 3A–D). To allow a quantitative analysis of the data, we first performed a pixel shift analysis of the TIRFM setup using TetraSpec fluorescent beads measured by TIRFM at 488 and 561 nm. The bead

Figure 1 STIM1, ORAI1 and PMCA4b localization at the IS. (**A**) Widefield deconvolution microscopy (WFDM) of an ORAI1–mEGFP (green) and STIM1–TagRFP-T (red) overexpressing Jurkat T cell contacting a SEE-pulsed Raji B cell, which was stained with fura-2/AM (blue) (see also Supplementary Movie S2). Displayed as XY maximum intensity projections (MIP), STIM1 co-accumulates with ORAI1 first in a cap-like structure distal to the contact point (IS) before being translocated together with ORAI1 to the IS. (**B**) Example of ORAI1 accumulation 60 min after contact with SEE-pulsed Raji cells (dotted lines). (i) Shown are four Jurkat T cells overexpressing ORAI1–mEGFP (green) and STIM1–TagRFP-T (red, the red channel overlaps with ORAI1 and is mostly visible as yellow, the cell with 'no accumulation' did not express STIM1). The line graphs depict fluorescence distribution in the yellow arrows. (ii) Examples of either ORAI1 stable expressing cells or endogenous antibody stained cells accumulating ORAI1 at the IS. (iii) Statistical analysis of ORAI1 accumulation phenotypes 60 min after contact with a SEE-pulsed Raji cell or an anti-CD3 antibody-coated bead (beads: $N = 13$ experiments, $n = 234$ cells; Raji: $N = 9$, $n = 203$; ORAI1 + STIM1 Raji: $N = 6$, $n = 109$; stable: $N = 4$, $n = 161$; endogenous: $N = 3$, $n = 91$, stable/endogenous ORAI1 P (distal) = 0.029, P (IS) = 0.03). (**C**) Contact between an EGFP–PMCA4b expressing Jurkat T cell and a SEE-pulsed Raji B-cell (blue). PMCA4b is enriched at the IS after contact (see in the picture taken 32 min after contact). (**D**) Phenotype examples of fixed cells stained for endogenous PMCA. (**E**) Statistical analysis of living and fixed cells like the ones shown in (**D**, **E**) (live: $N = 11$, $n = 76$; fixed: $N = 3$, $n = 91$). (**F**) Example of a cell fixed and stained with an antibody against SERCA 2 and 3. Scale bars are 10 μm.

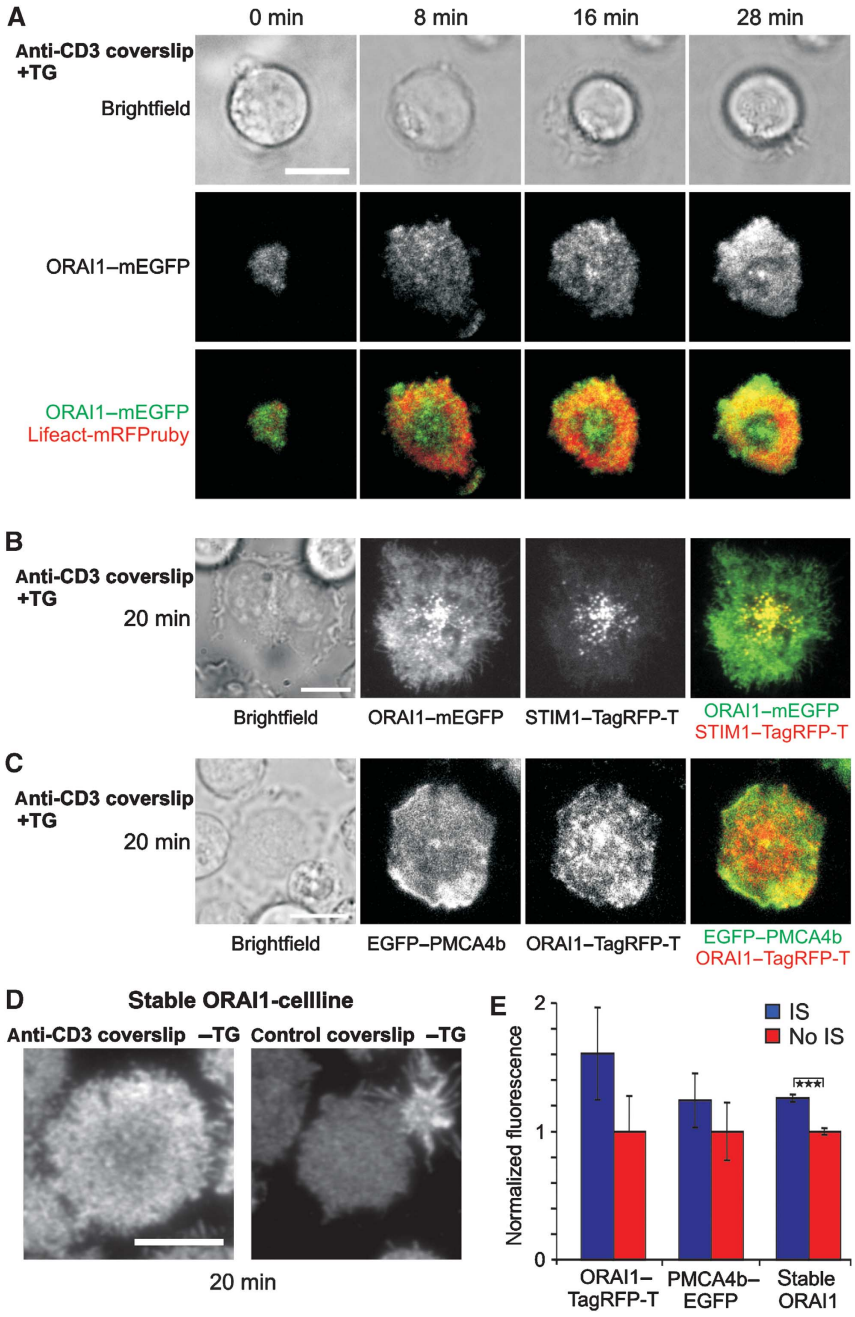

Figure 2 ORAI1, STIM1 and PMCA4b localization at the IS visualized with TIRFM. (**A**) TIRFM of an ORAI1–mEGFP and Lifeact-mRFPruby expressing Jurkat T cell stimulated with TG and settled on an anti-CD3 antibody-coated coverslip. Flattening of the cell and the ring-shaped actin accumulation (red) confirm formation of a stable IS. (**B**) TIRFM of an ORAI1–mEGFP and STIM1–TagRFP-T expressing Jurkat T cell stimulated with TG and settled on an anti-CD3 antibody-coated coverslip. (**C**) TIRFM of an EGFP–PMCA4b and ORAI1–TagRFP-T overexpressing Jurkat T cell stimulated with TG and settled on an anti-CD3 antibody-coated coverslip. (**D**) Phenotype examples of ORAI1 stable-expressing cells settled on either anti-CD3 or uncoated coverslips, fixed and stained with an antibody against ORAI1. (**E**) Statistical analysis of total ORAI1 or PMCA fluorescence from cells of (**C**, **D**) (ORAI1–TagRFP-T/PMCA4b–EGFP: n (IS) = 29, n (No IS) = 17; stable cell line n (IS) = 136, n (No IS) = 179, $P = 1.48 \times 10^{-10}$). Scale bars are 10 μm.

analysis confirmed the absence of pixel shifts in our TIRFM setup (data not shown). ORAI1–mEGFP expressing Jurkat T cells were loaded with MitoTracker® DeepRed and then plated onto anti-CD3 antibody-coated coverslips for 20 min. Merged pictures show that mitochondria do not co-localize with ORAI1 clusters, but are sitting next to them at the IS (Figure 3A). Similar results were obtained for mitochondria and ORAI3 channels (data not shown). The statistical analysis of the co-localization experiments illustrates the very low overlapping between ORAI1 clusters and mitochondria spots at the IS (Figure 3D). In contrast, PMCA and mitochondria show a higher co-localization at the IS (Figure 3B and D). Considering the co-localization results of mitochondria with ORAI1 and with PMCA, it is not surprising that the co-localization analysis between ORAI1 and PMCA at the IS revealed only a weak overlap (Figure 3C and D). Interestingly, ORAI1 channel clusters strongly overlap with PMCA following thapsigargin (TG) stimulation, which maximally activates

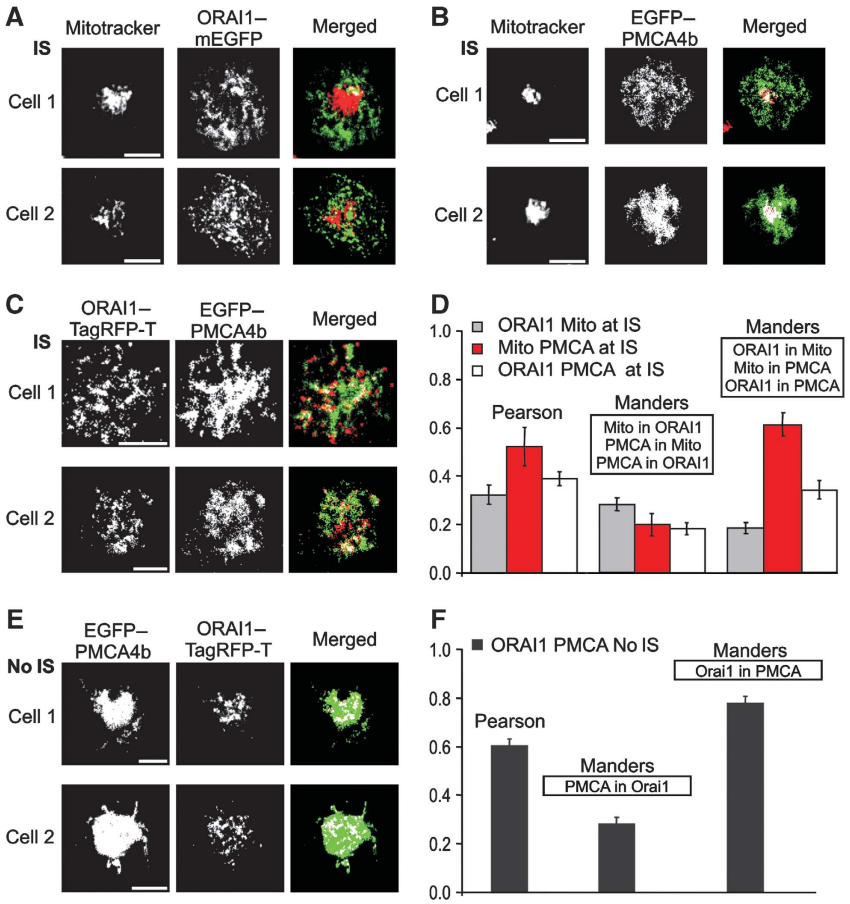

Figure 3 Mitochondria co-localize with PMCA but not with ORAI channels at the IS. (**A**) MitoTracker® DeepRed and ORAI1–mEGFP fluorescence pictures obtained by TIRFM with their corresponding merged pictures of two single representative Jurkat T cells 20 min after the formation of the IS. White points in merged pictures represent co-localization areas between mitochondria (red) and ORAI1 (green). (**B**) Same as in (**A**) for Jurkat T cells transiently expressing EGFP–PMCA4b. (**C**) Same as in (**A**) for T cells transiently expressing EGFP–PMCA4b and ORAI1–TagRFP-T. Scale bars are 5 μm. (**D**) Statistical analysis of co-localization between mitochondria and ORAI1 (grey, $n=20$), mitochondria and PMCA (red, $n=9$), and ORAI1 and PMCA (white, $n=13$) at the IS. Errors bars indicate s.e.m. (**E**) EGFP–PMCA4b and ORAI1–TagRFP-T fluorescence pictures obtained by TIRFM with their corresponded merged pictures of two single Jurkat T cells 20 min after Ca^{2+} influx activated with TG only. Cells were transiently co-expressing EGFP–PMCA4b and ORAI1–TagRFP-T. White points in merged pictures represent co-localization areas between PMCA (green) and ORAI1 (red). (**F**) Co-localization analysis between PMCA and ORAI1 (from **E**).

ORAI channels without inducing IS formation (Figure 3E and F). The better co-localization between ORAI1 and PMCA is due to the very homogenous distribution of PMCA following TG stimulation. This suggests that IS formation induces a re-distribution of PMCA from a more homogenous distribution into discrete regions of the PM at the IS. This re-localization decreases the co-localization with ORAI1 clusters but enhances the overlap with mitochondria.

Analysis of Ca^{2+} microdomains at the IS: T-cell activation requires low local Ca^{2+} signals controlled by subplasmalemmal mitochondria

Considering the dramatic polarization of proteins and organelles during IS formation, it is not surprising that localized signalling is very important for T-cell activation. While the importance of Ca^{2+} signals for T-cell activation is undisputed, nothing is currently known about local Ca^{2+} signals at the IS. Taking advantage of TIRFM, we analysed subplasmalemmal Ca^{2+} signals at the IS and the impact of mitochondria on Ca^{2+} signals beneath the IS. Mitochondrial localization at the subplasmalemmal area was compared in four different conditions: No IS (TG stimulation, which induces maximal activation CRAC/ORAI channels), IS (induced with anti-CD3 antibodies coated on coverslips) and both conditions in the presence of LFA stimulation, which was shown to be important for mitochondria localization at the IS by Contento *et al* (2010). The results are shown in Figure 4A. LFA stimulation alone had a small effect on the mitochondrial localization, whereas TCR stimulation through anti-CD3 antibodies induced mitochondria accumulation at the IS, which was further enhanced by LFA stimulation. To analyse Ca^{2+} signals at the IS, we loaded Jurkat T cells with Fluo-5F/AM (Figure 4B). Cells were pre-treated with TG in the absence of extracellular Ca^{2+} to maximally deplete Ca^{2+} stores and thereby maximally activate ORAI channels. At the same time, cells were plated onto coverslips coated with anti-CD3 antibodies to induce the formation of the IS or onto uncoated coverslips as control (No IS). After 10 min incubation, Ca^{2+}-containing solution (20 mM) was added to allow Ca^{2+} influx through ORAI channels and thereby activate mitochondrial translocation. Local Ca^{2+} signals at the membrane were measured with TIRFM and global cytosolic Ca^{2+} signals were measured in the same cells with epifluorescence (Figure 4B). Stimulation with TG in the absence of IS

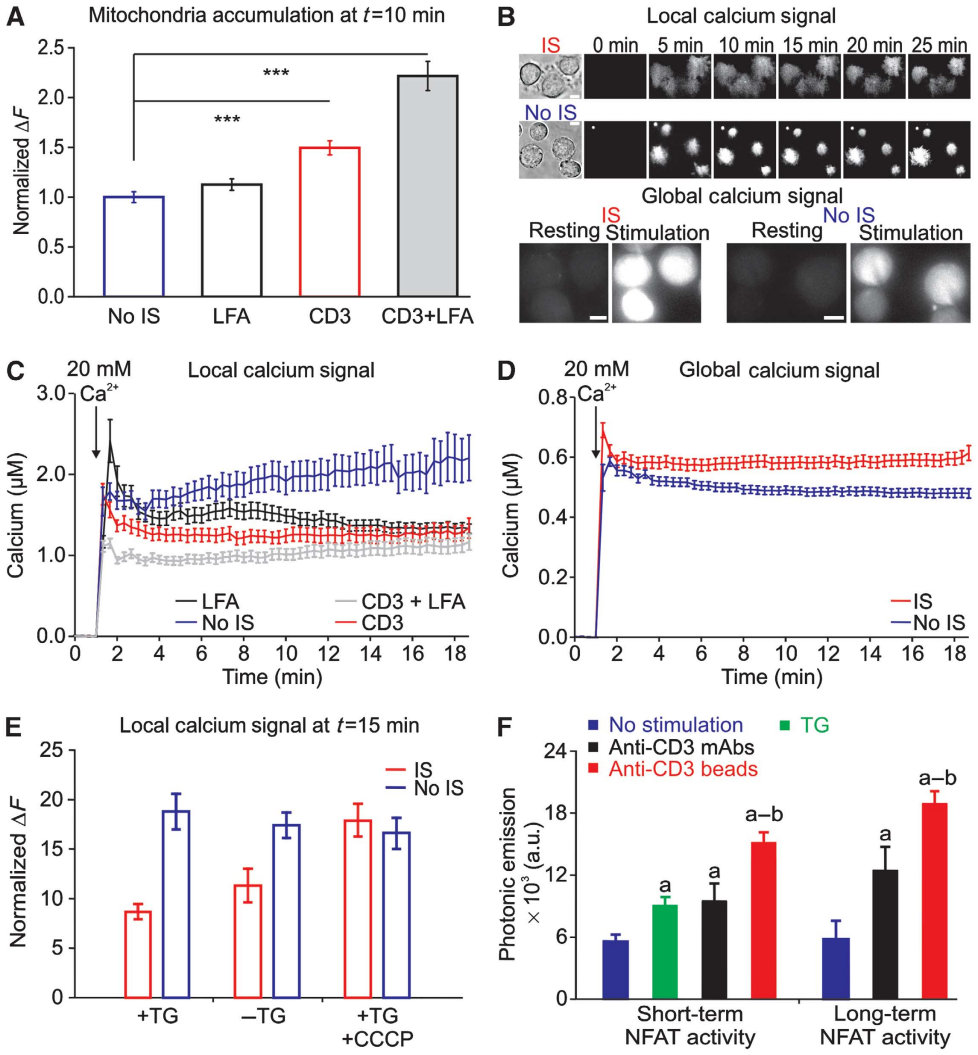

Figure 4 Formation of the IS induces mitochondrial accumulation, low subplasma membrane but high global Ca^{2+} signals and results in a larger NFAT activity. (**A**) Normalized TIRFM Mitotracker® green fluorescence 10 min after 20 Ca^{2+} addition from cells settled on either uncoated ($n=228$), activating LFA-1 ($n=149$), CD3 ($n=161$) or activating LFA-1 plus CD3 ($n=113$) antibody-coated coverslips. (**B**) Brightfield images (before Ca^{2+} addition) and TIRFM pictures of Fluo-5F/AM-loaded Jurkat T cells that were settled on either anti-CD3 antibody-coated coverslips (IS, top panel) or uncoated coverslips (No IS, bottom panel). Ca^{2+} stores were depleted by 10 min TG pre-treatment. Three minutes after starting the acquisition, cells were exposed to 20 mM Ca^{2+} for the next 22 min. Epifluorescence microscopy pictures of Fluo-5F/AM-loaded Jurkat T cells that were settled on either anti-CD3 antibody-coated coverslips (IS, top panel) or uncoated coverslips (No IS, bottom panel). (**C**) Local Ca^{2+} response measured by TIRFM from cells settled on either uncoated or coated coverslips with LFA-1, CD3 or LFA-1 plus CD3 antibodies (No IS $n=54$, LFA $n=59$, CD3 $n=28$, CD3 + LFA $n=37$). (**D**) Global Ca^{2+} responses from the same cells as in (**C**) ($P=0.0036$). (**E**) Mean normalized fluorescence $\Delta F=(100\times(F-F_0)/F_0)$) of Fluo-5F in TIRFM of Jurkat T cells upon IS (red columns) or No IS (blue columns) stimulation in the presence or absence of TG and in the presence of TG + CCCP as indicated (+TG n (IS) = 33, +TG n (No IS) = 37, $P<0.0001$; –TG n (IS) = 64, –TG n (No IS) = 40, $P<0.0001$, +TG +CCCP n (IS) = 126, +TG +CCCP n (No IS) = 99, $P=0.5795$). (**F**) Long-term measurements of NFAT activity in Jurkat T cells expressing luciferase under control of 3 × NFAT response elements treated with anti-CD3 antibody-coated beads, anti-CD3 antibodies, TG or untreated (no stimulation). Mean values of photonic emissions reflecting NFAT activity released at 14 (long-term activity) and 6 (short-term activity) hours were calculated after no treatment (no stimulation), anti-CD3 mAbs, anti-CD3 antibody-coated beads and TG ($n=6$ experiments; $a=P<0.05$ versus no stimulation; $b=P<0.05$ versus anti-CD3 mAbs). Errors bars indicate s.e.m. Scale bars are 5 μm.

formation (No IS) induced the highest local Ca^{2+} concentration, whereas IS formation decreased the local Ca^{2+} signals (Figure 4B and C). CD3 ± LFA stimulation showed the largest mitochondrial accumulation (Figure 4A) and the smallest local Ca^{2+} signals (Figure 4C). Thus, local Ca^{2+} signals in T cells correlated inversely with the mitochondrial accumulation at the PM. However, in the same cells, global Ca^{2+} signals were significantly higher in IS-stimulated T cells than in T cells following only TG stimulation (Figure 4D). This means that more Ca^{2+} must be transported from the local Ca^{2+} domain deep into the cytosol after IS formation compared with No IS stimulation (TG only). The global Ca^{2+} concentrations measured with Fluo-5F are by a factor of 2 lower than the Ca^{2+} concentrations we have measured previously with Fura-2 using an epifluorescence video-imaging system (Quintana *et al*, 2007, 2009). This may be a problem of the *in vitro* calibration we had to perform for Fluo-5F with the TIRFM setup because we could technically not perform a calibration for each cell, which is in our opinion required for a reliable *in vivo* calibration with a single wavelength dye.

The measurements shown in Figure 4C and D require the constant switching between TIRF and epifluorescence mode, which is not ideal. We thus repeated the local Ca^{2+} measurements under the same conditions but without measuring global Ca^{2+} in the same cells. Normalization of Fluo-5F signals ($\Delta F = 100 \times ((F-F_0)/F_0)$ of the first two bars in Figure 4E shows the same result as in Figure 4C, comparing local Ca^{2+} plateaus in the presence of TG 15 min after activating Ca^{2+} entry. Local Ca^{2+} is reduced following IS stimulation compared with No IS. Similar results were observed with Fluo-4FF (data not shown). Again, local Ca^{2+} signals were decreased at the IS compared with No IS, whereas global Ca^{2+} signals were enhanced following IS formation on average by a factor of 1.4 (with Fluo-5F) or even 3 (with Fluo-4FF). To investigate a potential involvement of SERCA in regulating local Ca^{2+} domains at the IS, we next tested if TG influences local Ca^{2+}. Ca^{2+} entry can be also activated by incubating T cells for several minutes without external Ca^{2+} and no other stimulus present because Ca^{2+} pools will slowly be depleted under these conditions (data not shown). With no TG present, we measured the same local Ca^{2+} signals (Figure 4E). Again, IS formation reduced the local Ca^{2+} signals. This result indicates that SERCA activity does not play a major role for controlling local Ca^{2+} signals at the IS.

Because the local Ca^{2+} concentration at the IS correlated with the presence of mitochondria, it is expected that the inhibition of mitochondrial Ca^{2+} uptake should influence local Ca^{2+} signals. We tested this with the addition of CCCP, which collapses the mitochondrial membrane potential and thereby inhibits mitochondrial Ca^{2+} uptake by disrupting the Ca^{2+} driving force for Ca^{2+} entry into mitochondria (Supplementary Figure S2A). In the presence of CCCP, the sustained local Ca^{2+} concentration following IS formation is indeed now similar to the local Ca^{2+} concentration if cells are stimulated with TG only (No IS) (Figure 4E). These experiments indicate that mitochondrial Ca^{2+} uptake influences local Ca^{2+} signals at the IS. In addition, these experiments also rule out that the Ca^{2+} signals that we measure at the IS are influenced by the mitochondrial space, which could decrease the amount of Fluo-5F at the IS.

At a first glance it may be surprising that SERCA Ca^{2+} uptake does not influence local Ca^{2+} signals at the IS while mitochondrial Ca^{2+} uptake does. Considering the low transport rates of SERCA compared with the large transport rates of the mitochondrial Ca^{2+} uniporter (Baughman *et al*, 2011; De Stefani *et al*, 2011), this result is not unexpected at all. In addition, we did not observe any accumulation of SERCA at the IS (Figure 1F) while mitochondria accumulated at the IS (Figure 4A).

Our Ca^{2+} measurements suggest that efficient Ca^{2+}-dependent activation of T cells under physiological stimulation (following IS formation) requires low local Ca^{2+} signals. Indeed, both short- and long-term measurements of Ca^{2+}-dependent nuclear factor of activated T cells (NFAT) activity revealed that IS stimulation induces the largest NFAT translocation into the nucleus (Figure 4F).

Subplasmalemmal mitochondria control local Ca^{2+} distribution at the IS

To analyse the influence of mitochondria on the local Ca^{2+} signals at the IS, we co-loaded T cells with Fluo-5F/AM and MitoTracker® DeepRed/AM. Cells were pre-treated and stimulated as explained before. Figure 5A shows that Ca^{2+} signals in mitochondrial areas are significantly lower than in areas free of mitochondria 20 min after IS formation. A similar inverse correlation was found by plotting the normalized fluorescence of Fluo-5F and MitoTracker® DeepRed of individual cells against each other (Figure 5B). Considering the different Ca^{2+} concentrations in mitochondrial and non-mitochondrial areas, it is not surprising that a spatially resolved surface plot analysis revealed very heterogeneous $[Ca^{2+}]_i$ profiles at the IS. In TG-treated cells (No IS), however, these heterogeneous $[Ca^{2+}]_i$ profiles were not observed (Figure 5C and D). A quantification of the Ca^{2+} heterogeneity in the presence or absence of an IS was done by calculating the coefficient of variation (CV). An increase in the CV indicates that the spatial signal fluctuations are increasing in relation to the mean signal, suggesting a higher heterogeneity of the signal. The analysis of CV over time illustrates that fluorescence heterogeneity is more pronounced after IS formation following Ca^{2+} influx (Figure 5E and F). Greater statistical differences were obtained with the Ca^{2+} indicator Fluo-4FF because of its lower affinity for Ca^{2+} ($K_d = 9.7\,\mu M$) compared with Fluo-5F ($K_d = 2.3\,\mu M$). Taken together, we conclude that the accumulation of mitochondria strongly modulates local Ca^{2+} signals at the IS.

Mitochondria at the IS modulate the Ca^{2+} microdomain-dependent PMCA activity

PMCA activity has been reported to be modulated by global cytosolic Ca^{2+} signals but also by local Ca^{2+} microdomains generated beneath open ORAI channels (Bautista *et al*, 2002; Bautista and Lewis, 2004). Our analysis of local Ca^{2+} signals at the IS predicts that PMCA modulation should be influenced after IS formation. Using a previously described experimental approach (Bautista and Lewis, 2004) (details are explained in the Supplementary data and Supplementary Figure S3), we analysed the Ca^{2+} microdomain-dependent modulation of PMCA activity in the presence or absence of IS.

Ca^{2+} influx was activated by TG alone (No IS) or with a combination of TG and anti-CD3 antibody-coated beads (IS). To determine PMCA modulation, Ca^{2+} influx was activated in the presence of 1 mM external Ca^{2+} (Ca_o^{2+}) and subsequently in the presence of 20 mM external Ca^{2+} (Figure 6A and B). As introduced by Bautista *et al* (2002) and Bautista and Lewis (2004) and in detail explained in the Supplementary data, we only analysed cells that displayed similar Ca^{2+} plateaus in 1 and 20 mM external Ca^{2+}, so-called iso-cells. Figure 6A depicts the average response to 1 and 20 mM Ca_o^{2+} of iso-cells following TG stimulation or IS formation in Jurkat T cells, respectively. As has been reported previously for TG-stimulated T cells (No IS), 20 mM Ca_o^{2+} significantly elevated the clearance rate in every cell by an average of 1.6 ± 0.03 a.u./s compared to those rates measured in 1 mM Ca_o^{2+} despite the same steady-state global $[Ca^{2+}]_i$ (Bautista *et al*, 2002; Bautista and Lewis, 2004). Since CRAC/ORAI1 channels conduct more Ca^{2+} in 20 mM Ca_o^{2+} than in 1 mM Ca_o^{2+}, Ca^{2+} export needs to be enhanced if global $[Ca^{2+}]_i$ is in steady state. Bautista and Lewis (2004) demonstrated that this can only be explained by the contribution of local Ca^{2+} microdomains to PMCA modulation whose extent and/or magnitude are modulated by Ca_o^{2+}. In contrast, IS formation completely abrogated the Ca^{2+}

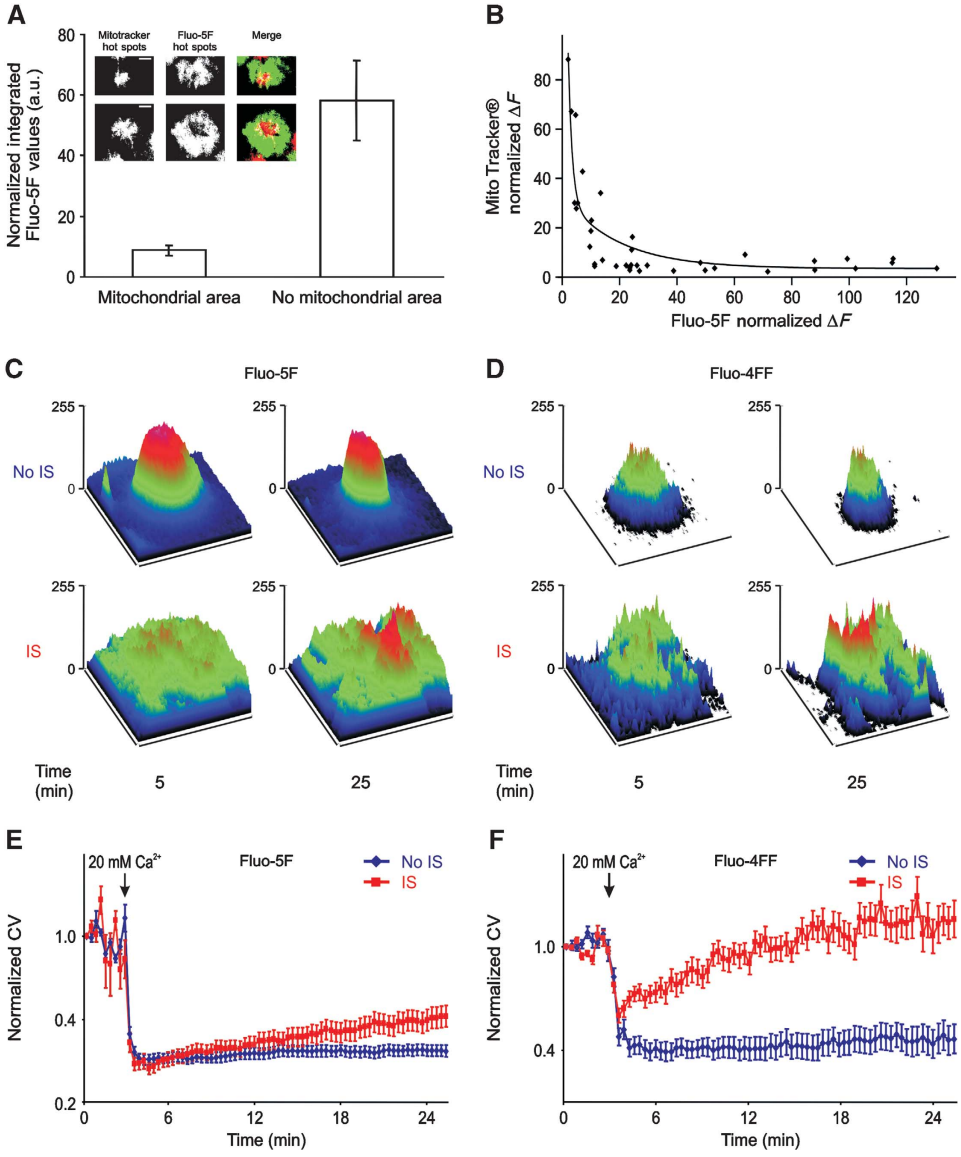

Figure 5 Mitochondria at the IS reduce subplasma membrane Ca^{2+} signals and increases their heterogeneity. (**A**) Average of normalized integrated Fluo-5F values after 20 min of IS formation from intracellular areas at the IS where mitochondria either localize or do not localize ($n=20$ cells and 40 mitochondria spots, $P<0.01$). Insets show pictures of hot areas of MitoTracker® DeepRed and Fluo-5F fluorescence with the corresponding merged pictures of two single 5F/AM- MitoTracker® Green/AM co-loaded Jurkat T cells 20 min after IS formation on anti-CD3 antibody-coated coverslips in the presence of 20 mM $[Ca^{2+}]_o$ solution. Hot areas are defined as the areas with the highest MitoTracker® DeepRed and Fluo-5F fluorescences. (**B**) Normalized MitoTracker® fluorescence in single cells as a function of normalized Fluo-5F fluorescence from the co-loaded cells analysed in (**A**). (**C**, **D**) Surface plots of subplasmalemmal Ca^{2+} signals from single representative Fluo-5F/AM (**C**) or Fluo-4FF/AM (**D**) -loaded T cells at 5 and 25 min after TG stimulation (top panel, No IS) or IS formation (bottom panel). (**E**, **F**) Average of normalized CV from Fluo-5F (**E**) and Fluo-4FF (**F**) fluorescence at subplasma membrane regions in T cells stimulated with TG (No IS, blue traces) or upon IS formation (red traces) over time ($n=63$, $P<0.01$; $n=47$, $P<0.001$). Errors bars indicate s.e.m. Scale bars are 5 μm.

microdomain-dependent upregulation of PMCA activity (clearance rate difference was 1.1 ± 0.09 a.u./s between 20 and 1 mM external Ca^{2+} (Figure 6A, red trace). Comparable results were obtained in human $CD4^+$ T cells (Figure 6B) only that Ca_o^{2+} was elevated from 1 to 5 mM (and not to 20 mM) to avoid saturation of Fura-2 as human T lymphocytes display higher Ca^{2+} signals than Jurkat T cells. To explain these observations, we suggest the following hypothesis: mitochondrial accumulation in the immediate vicinity of the IS prevents local Ca^{2+}-dependent modulation of PMCA activity. This hypothesis is in full agreement with our finding that Ca^{2+} microdomains at the IS are smaller than at the PM following TG stimulation.

Bautista *et al* (2002) and Bautista and Lewis (2004) have shown that the iso-cell analysis is not restricted to a subset of T cells. Nevertheless, we analysed subsets of cells in different phases of the cell cycle. Cells were arrested in different phases as confirmed by DAPI staining (Supplementary Figure S4A). Analysing Ca^{2+} extrusion rates similarly as shown in Figure 6A, we found again that up-modulation of the PMCA was reduced by IS formation (Supplementary Figure S4B), in G_1 and S/G_2 more drastically than in G_1/S.

Although our PMCA modulation analysis supports our hypothesis about the main role of subplasmalemmal mitochondria to control local Ca^{2+} signals and Ca^{2+}-dependent processes at the IS, we also performed a set of TIRFM

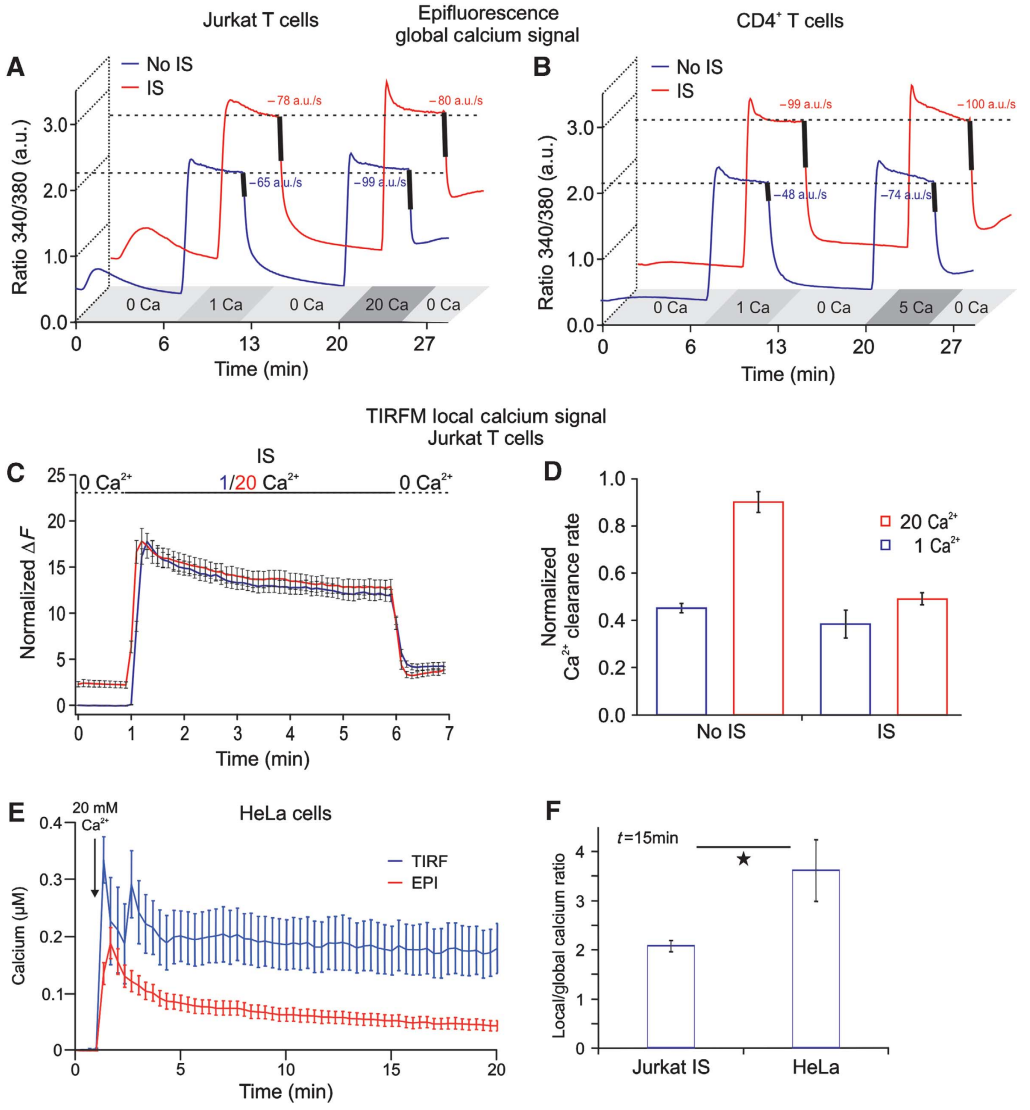

Figure 6 Formation of the IS reduces Ca^{2+} microdomain-dependent modulation of PMCA activity in Jurkat T cells. (**A**) Average of $[Ca^{2+}]_i$ responses of so-called iso-cells induced by 1 or 20 mM extracellular Ca^{2+} solutions in Jurkat T cells. The averages of Ca^{2+} clearance rates following $[Ca^{2+}]_i$ elevation, indicated by the thick lines, were calculated from the dRatio (340/380)/d*t* slopes over 10 s periods following $[Ca^{2+}]_o$ removal (n (No IS) = 180, $P < 0.001$; n (IS) = 60, $P = 0.76$). (**B**) Same experiments and analysis as in (**A**) only with human $CD4^+$ T cells in the presence of 1 or 5 mM extracellular Ca^{2+} solutions to avoid saturation of the system (n (No IS) = 253, $P < 0.001$; n (IS) = 176, $P = 0.6$). (**C**, **D**) Same experimental design and analysis as in (**A**) only with TIRFM (n (IS) = 18, n (No IS) = 50). (**E**) Global (red trace) and local (blue trace) Ca^{2+} signals of Fluo-5F-loaded HeLa cells in response to TG stimulation in the presence of 20 mM extracellular Ca^{2+} solution. Global Ca^{2+} signals were measured by epifluorescence while local signals were obtained by TIRFM in the same cells. (**F**) Ratio between the local and global Ca^{2+} response at 15 min after stimulation with TG in HeLa cells or with TG plus IS in Jurkat T cells. HeLa data were obtained from two independent experiments ($n = 12$, $P = 0.037$). Jurkat T-cell data were taken from experiments shown in Figure 4C and D.

experiments to analyse the local Ca^{2+} domains. We compared local Ca^{2+} signals generated by 1 and 20 mM Ca^{2+} solutions at the TIRF layer in the same cell following IS formation. The increase in Ca_o^{2+} will enhance the Ca^{2+} driving force and thereby generating larger Ca^{2+} influx. Figure 6C shows that local Ca^{2+} signals at the IS were independent of the extracellular Ca^{2+} solution because sustained Ca^{2+} microdomains generated by 1 and 20 mM Ca^{2+} solutions are similar in size following IS formation. We next tested the pump rates in TIRFM experiments and found no significant difference in the Ca^{2+} clearance rate of cells exposed to 1 and 20 mM Ca^{2+} solution following IS formation (Figure 6D). However, in the absence of IS (TG stimulation), PMCA modulation was present as seen before (Figure 6D, compare also with Figure 6A and B). Taken together, these results imply that mitochondria, through adapting their position at the IS and/or their amount of Ca^{2+} uptake, control the amplitude of the local Ca^{2+} microdomain at the IS and the global cytosolic Ca^{2+} signal.

From the data of Giacomello *et al* (2010), it is clear that mitochondria do not control store-operated Ca^{2+} entry in HeLa cells. This cell line is therefore a good 'control' for the mitochondria PM interaction that we found for the IS. We thus tested how much of the local Ca^{2+} concentration generated by store-operated Ca^{2+} entry was 'translated' into a global Ca^{2+} signal in HeLa cells. Figure 6E and F depicts local and global Ca^{2+} measurements following TG stimulation in the same HeLa cells. Comparing now the ratio

between local and global Ca^{2+} in these cells with IS-forming Jurkat T cells, it is obvious that HeLa cells are very inefficient to transport local Ca^{2+} from the membrane into the cytosol because their local Ca^{2+} signal is very large in relation to their global Ca^{2+} signal (Figure 6F). This is different in T cells. Thus, we confirm the data by Giacomello *et al* (2010) that mitochondria do not control SOCE in HeLa cells. In T cells, however, mitochondria are much more dynamic and can adapt to the need of the immune synapse.

Although we found strong correlations between the amount of mitochondria at the IS and the local Ca^{2+} signal and subsequent PMCA modulation, we still wanted to disrupt mitochondrial localization at the IS without influencing ORAI1-dependent Ca^{2+} entry. By using cytoskeleton poisoning drugs (nocodazole, latrunculin A and B, cytochalasin D), we abrogated the cytoskeleton-dependent mitochondrial translocation to the IS. Importantly, the drugs do not affect CRAC/ORAI channel activity, pump rates, mitochondrial Ca^{2+} uptake, Ca^{2+}-dependent K^+ channel and Ca^{2+} release following formation of the IS (Quintana *et al*, 2006; Supplementary Figure S2). This implies that the entire Ca^{2+} influx and Ca^{2+} release processes are not altered by these drugs.

In case of nocodazole, a tubulin polymerization-disrupting drug, the recruitment of actin filaments (Figure 7A) and subsequent TCR accumulation (data not shown) to the IS, which are considered a hallmark for the formation of a matured IS, were not affected (Figure 7A), indicating that a functional IS was formed. In case of actin poison drugs, the situation was slightly different because the abrogation of actin polymerization disrupts of course IS formation (Figure 7A) and thereby the accumulation of mitochondria into the vicinity of IS. But the final result was the same as that obtained with nocodazole treatment because CRAC/ORAI channels, STIM1 and PMCA undergo a normal endoplasmic reticulum (ER) and PM re-arrangement following TG stimulation as previously reported (Bakowski *et al*, 2001; Quintana *et al*, 2006, 2007, 2009). The ORAI fluorescence at the TIRF layer and the ORAI fluorescence measured with epifluorescence were not significantly altered. In other words, actin is not required for STIM1–ORAI1-dependent Ca^{2+} influx upon TG stimulation (Bakowski *et al*, 2001; Mueller *et al*, 2007) (Supplementary Figure S2). Therefore, if one co-stimulates latrunculin or cytochalasin D-treated cells with antibodies-coated coverslips and TG, then cells should respond the same as No IS-stimulated cells (Quintana *et al*, 2007). Thus, in the absence of actin polymerization, mitochondria are not able to accumulate beneath the IS (Figure 8A and B), even though Ca^{2+} influx through CRAC/ORAI channels is ensured by TG stimulation (Bakowski *et al*, 2001; Mueller *et al*, 2007) (Supplementary Figure S2) in addition to focal stimulation through the beads.

As shown in Figure 8, the abrogation of mitochondrial translocation to the TIRF layer by cytoskeleton-disrupting drugs (Figure 8A and B) correlated with the presence of local PMCA modulation (Figure 8C–F). Most important is here the nocodazole experiment, because under these conditions there is still a functional IS formed. The increase of the Ca^{2+} clearance rate in the presence of cytoskeleton poisons compared with the control experiment (Figure 8G) is explained by the augmentation of local Ca^{2+} signals because of the absence of subplasmalemmal mitochondria (Figure 8A and B). This was directly proven by measurements of local Ca^{2+} influx in latrunculin B-treated cells. Interfering with actin polymerization generated local Ca^{2+} signals similar to control cells (Figure 8H). Overall, we can conclude that mitochondrial positioning relative to CRAC/ORAI channels is essential to control Ca^{2+} microdomains beneath the IS and the subsequent PMCA modulation.

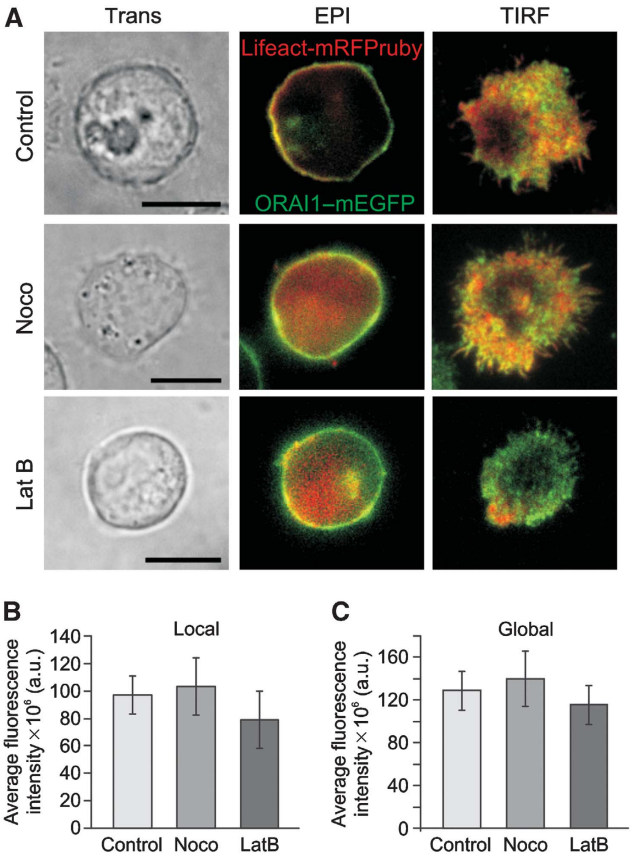

Figure 7 Cytoskeleton polymerization-disrupting drugs do not inhibit ORAI accumulation at the IS. (**A**) Transmission light (Trans), epifluorescence (Epi) and TIRFM pictures of representative single Jurkat T cells treated with cytoskeleton-disrupting drugs (2 μM nocodazole, 10 μg/ml latrunculin B). Cells were transiently expressing Lifeact-mRFPruby and ORAI1–mEGFP proteins. After treatment, T-cells were settled on anti-CD3 antibody-coated coverslips for 20–30 min in the presence of extracellular Ca^{2+} solution to induce the formation of a matured IS. Scale bars are 10 μm. Average intensity of the local (**B**) and global (**C**) fluorescence signal of ORAI1–mEGFP measured for cells pre-treated with nocodazole or latrunculin B or kept under control conditions (control $n = 32$, nocodazole $n = 20$, latrunculin B $n = 21$).

A mathematical model predicts the dependence of global Ca^{2+} concentrations on local Ca^{2+} concentrations at the IS as a function of the distance between IS and mitochondria

At this point, our model that mitochondrial positioning controls the local and global Ca^{2+} concentrations at the IS has been tested by two independent lines of evidence: TIRF measurements of local Ca^{2+} and PMCA modulation analysis. As a final independent method to test the dependence of global Ca^{2+} concentrations on local Ca^{2+} concentrations controlled by mitochondria positioning, we developed a simplified mathematical model of the different Ca^{2+} trans-

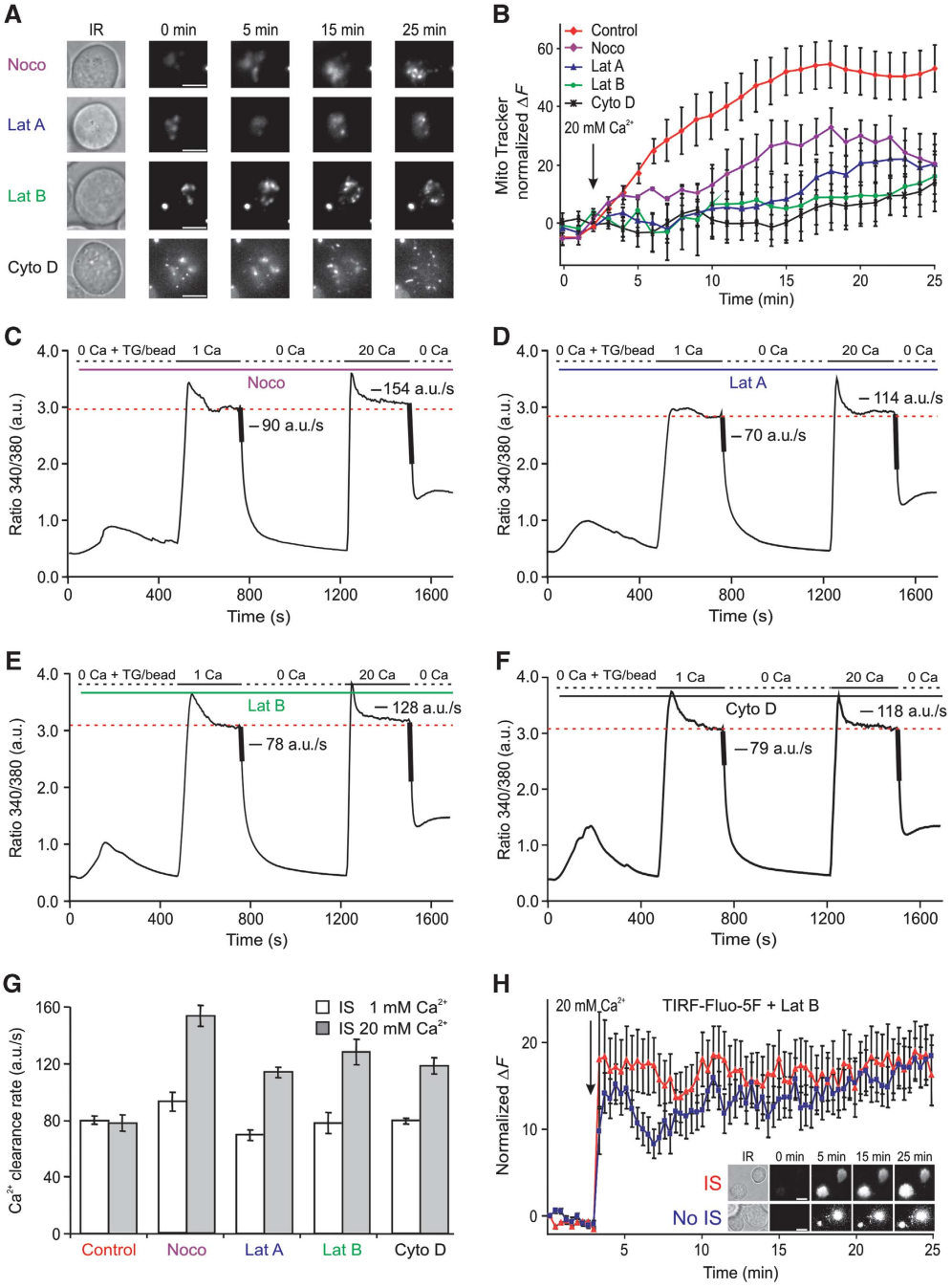

Figure 8 Disruption of cytoskeleton-dependent mitochondrial translocation to the IS rescues the Ca^{2+} microdomain-dependent modulation of PMCA activity. (**A**) Brightfield images (before stimulation) and TIRFM images of single representative MitoTracker® Green/AM-loaded Jurkat T cells that were pre-treated with nocodazole (2 μM) latrunculin A (10 μg/ml), latrunculin B (10 μg/ml) or cytochalsin D (10 μM) as indicated in order to block the cytoskeleton-dependent mitochondrial translocation to the IS. Cells were settled on anti-CD3 antibody-coated coverslips (IS) for 5–7 min in a Ca^{2+}-free solution to induce the maximal depletion of intracellular Ca^{2+} stores. Three minutes after starting the acquisition, cells were exposed to 20 mM Ca^{2+} for the next 22 min. The brightest point in the TIRFM picture belongs to a fluorescent bead (Invitrogen) used as control of the focus (see Materials and methods). (**B**) Statistical analysis of the normalized MitoTracker® fluorescence from 40 (Control, red trace), 10 (Noco, purple trace), 20 (Lat A, blue trace), 20 (Lat B, green trace) and 16 (Cyto D, black trace) cells analysed as the ones shown in (**A**) (Noco, Lat A, Lat B and Cyto D versus control at 20 min; $P=0.079$, $P=0.041$, $P=0.029$, $P=0.028$). (**C**, **F**) Average $[Ca^{2+}]_i$ responses and Ca^{2+} clearance rates from control iso-cells induced by 1 or 20 mM extracellular Ca^{2+} solutions in the presence of nocodazole (**C**), latrunculin A (**D**), latrunculin B (**E**) and cytochalasin D (**F**) following IS formation. Average Ca^{2+} clearance rates following $[Ca^{2+}]_i$ elevation (indicated by the thick lines) were calculated by the dRatio (340/380)/d*t* slopes over 10 s periods following external Ca^{2+} removal. (**G**) Statistical analysis of Ca^{2+} clearance rates from the cells shown in (**C**, **F**) compared with controls cells from Figure 6A (1 versus 20; control: $n=60$, $P=0.76$; Noco: $n=14$, $P<0.0001$; Lat A: $n=20$, $P<0.0001$; Lat B: $n=15$, $P<0.001$; Cyto D: $n=12$, $P<0.0001$). (**H**) Normalized Fluo-5F fluorescence from 15 (IS, red Δ) and 23 (No IS, blue □) cells, respectively (at 20 min, $P=0.6$). Inset shows brightfield images (before stimulation) and TIRFM pictures of Fluo-5F/AM-loaded Jurkat T cells. Cells were settled on either anti-CD3 antibody-coated coverslips (IS) or poly-L-ornithine-coated coverslips (No IS) in the absence of extracellular Ca^{2+} solution containing 1 μM TG for 5–7 min. Cells were pre-treated with latrunculin B (Lat B) as in (**A**). Three minutes after starting the acquisition, cells were exposed to 20 mM Ca^{2+} for the next 22 min. Errors bars indicate s.e.m. Scale bars are 5 μm.

port mechanisms. The influence of mitochondrial localization within the cytosol relative to the IS on the spatial distribution of Ca^{2+} was tested in the presence of open CRAC channels and blocked SERCA pumps (implying empty Ca^{2+} stores and continuous activation of CRAC channels). Since we expected the distance between the opened CRAC channels and the mitochondria to be the dominant physical determinant of the spatial Ca^{2+} distribution in this situation, we reduced the model to one spatial dimension, that is, a single variable x varying between $x=0$ (position of the IS with activated CRAC channels) and $x=L$ (position opposite to the IS, location of PMCA pumps away from the IS). Mitochondria occupy the region between x_{in} and x_{out}, and for simplicity, we consider a situation in which Ca influx has already saturated all buffers and that mitochondria only redistribute Ca^{2+}. We assume that the whole Ca^{2+} absorption capacity of the mitochondria is focused at position x_{in}, and that all Ca^{2+} absorbed at x_{in} is re-injected at position x_{out}. It is straightforward to generalize the model to continuous distributions of sources and sinks—here we stick to the simplest version since it is sufficient to understand the basic mechanisms.

Since PMCA are found at the IS and away from the IS, we located PMCA pumps close to the IS (at $x=x_0$, where $x_0=100$–200 nm) and at the opposite end of the cell (at $x=L$). In a one-dimensional model, there is no lateral direction, for which reason we have to place the mathematical representation of this PMCA behind the CRAC channel into the cytosol. The physical effect is the same as a sink located laterally in close distance: The Ca^{2+} concentration in the IS microdomain will be reduced.

We assume that all channel capacities and rates are constant and pump rates are linearly depended on the local Ca^{2+} concentration. The model and the expected spatial dependence of the Ca^{2+} concentration are sketched in Figure 9A (mathematical representation in Supplementary data). When no mobile buffers are present, cytosolic Ca^{2+} is freely diffusing, with sources and sinks as described above. Mathematically, this problem is described by a one-dimensional diffusion equation with sources, sinks and appropriate boundary conditions, which is solved in the Supplementary data. In Figure 9B, the Ca^{2+} concentration is shown as a function of x for different positions x_{in}, which is the distance between IS and mitochondria. As expected, the Ca^{2+} concentration at the IS decreases with decreasing the distance between IS and mitochondria, whereas the global Ca^{2+} concentration away from the IS increases. The effect is most pronounced for high mitochondrial uptake rates, where also the Ca^{2+} concentration at the IS is lowest. In Figure 9C, we compare the average Ca^{2+} concentration in the IS microdomain with the average global Ca^{2+} concentration, c_{global}. Clearly, Ca^{2+}_{IS} increases monotonically with the distance x_{in} of the mitochondria from the IS, whereas c_{global} decreases monotonically. Using this simple model, we have demonstrated that mitochondria relocation to the IS is sufficient to increase global Ca^{2+} concentrations. One might have expected that moving a strong sink closer to the main Ca^{2+} source will decrease the Ca^{2+} here and that the release of this absorbed Ca^{2+} at a distant site will increase the Ca^{2+} concentration there. But that the *total* amount of Ca^{2+} present in the cell will be substantially *increased* already by this simple re-distribution without any further mechanisms involved appears to be a rather non-trivial prediction of this simple model. In conclusion, the model predicts the dependence of global Ca^{2+} on local Ca^{2+} as a function of the distance between mitochondria and IS. If mitochondria are far away from the PM (No IS; Figure 4), the local Ca^{2+} concentration is high and the global one low, which is inverted if mitochondria are close to the PM in case the IS is formed (Figure 4).

Discussion

The sustained signalling required for efficient T_h-cell activation is achieved through the formation of a matured IS, a highly organized molecular mechanism that allows the integration of local PM receptor stimulation into sustained cell activation and differentiation (Dustin and Cooper, 2000). In this study, we have shown that the IS controls Ca^{2+} microdomains around ORAI channels with a mechanism that is optimized for T-cell activation. This is achieved by bringing mitochondria and ORAI channels into close proximity ($\sim$200 nm) and by re-organizing PMCA into discrete regions of the PM where they are co-localized with mitochondria at the IS. The protein and organelle re-distribution allows mitochondria to rapidly take up the inflowing Ca^{2+}, thereby avoiding high Ca^{2+} microdomains close to ORAI channels, which prevents Ca^{2+}-dependent channel inactivation and reduce local Ca^{2+}-dependent PMCA modulation. This optimizes net Ca^{2+} influx at the IS. By slowly exporting Ca^{2+} further away from the PM, mitochondria sustain an elevated global Ca^{2+} signal that enhances the translocation of NFAT into the nucleus and the subsequent activation of T_h cells.

The positioning of mitochondria close to ORAI channel clusters ($\sim$200 nm) is in a good agreement with the nanoscale molecular activation model of ORAI channels (Lewis, 2007). Following store depletion, STIM1 proteins accumulate in pre-existing and newly created discrete subregions of junctional ER located 10–25 nm from the PM. At the same time, ORAI proteins accumulate in regions of the PM directly opposite to the STIM1 clusters (also called puncta). Only ORAI channels in direct contact with STIM1 can be activated (Feske, 2007; Oh-hora and Rao, 2008). This protein–protein interaction precludes the localization of mitochondria directly beneath activated ORAI channel clusters. Very recently, the absence of co-localization between STIM1 puncta and subplasmalemmal mitochondria has been reported (Korzeniowski *et al*, 2009), which is in agreement with our results.

The mitochondrial control of CRAC/ORAI channels has been found to be important under physiological conditions of weak intracellular Ca^{2+} buffering (1.2 mM EGTA) but not in the presence of high concentration of Ca^{2+} chelator (10 mM EGTA) (Gilabert and Parekh, 2000; Hoth *et al*, 2000; Gilabert *et al*, 2001; Glitsch *et al*, 2002; Quintana *et al*, 2006). From these results, the size of Ca^{2+} microdomains that induces the slow Ca^{2+}-dependent inactivation of ORAI channels can be predicted. The mean path length that a Ca^{2+} ion travels before being intercepted by a buffer molecule is given by λ ($\sqrt{D_{ca}/k_{on}B}$). It depends on the chelator's on-rate k_{on}, the free buffer concentration B and the Ca^{2+} diffusion coefficient D_{ca} (Neher, 1998). Both D_{ca} and k_{on} are constants but buffer concentrations may change. While 10 mM of EGTA starts to intercept Ca^{2+} at 136 nm, 1.2 mM starts to buffer Ca^{2+} at

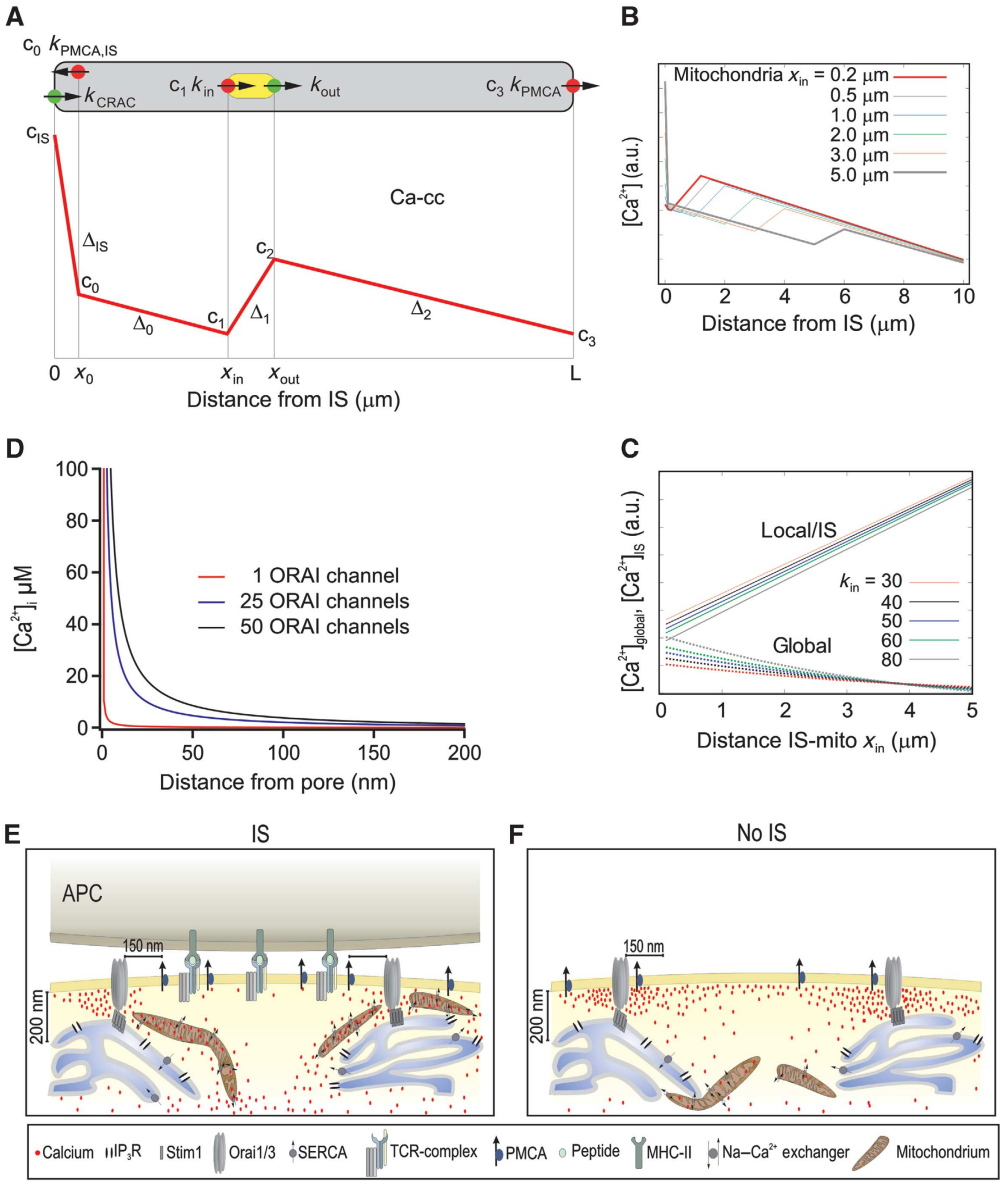

Figure 9 Mathematical model for the spatial arrangement of CRAC channels, mitochondria and PMCAs and the dependence of Ca^{2+} concentrations on the distance between IS and mitochondria (**A**) Overview over the one-dimensional model: cytosol is grey, mitochondria are yellow, Ca^{2+} sources are green and Ca^{2+} sinks are red. The red curve represents the expected spatial profile of the cytosolic Ca^{2+} concentration. c_{IS} is the concentration at the location of the CRAC channel ($x=0$), c_0 ca. 100 nm away from the CRAC channel (at x_0), c_1 at the front end of the mitochondria ($x=x_{in}$), c_2 at the back end ($x=x_{out}$) and c_3 at the PMCA pumps away from the IS ($x=L$). The slopes of the linear parts are denoted as Δ_{IS}, Δ_0, Δ_1 and Δ_2 (see Supplementary data). (**B**) Stationary Ca^{2+} concentration $c_s(x)$ as a function of x for different positions x_{in} of the mitochondria. The parameters are $k_{CRAC}=200/s$, $k_{in}=60\,\mu m/s$, $k_{PMCA}=20\,\mu m/s$, $k_{PMCAI,S}=40\,\mu m/s$. Note that parameters and concentrations are given in one-dimensional units, the three-dimensional equivalent can be computed with formula 10 in the Supplementary data. (**C**) Comparison of the stationary local Ca^{2+} concentration at the IS, c_{IS} (upper curves) and the average global Ca^{2+} concentrations c_{global} (lower curves) as a function of the distance x_{in} between IS and mitochondria for mitochondrial input rates k_{in}. The parameters are $k_{CRAC}=200/s$, $k_{in}=30$–$80\,\mu m/s$, $k_{PMCA}=20\,\mu m/s$, $k_{PMCAI,S}=40\,\mu m/s$. Note that parameters and concentrations are given in one-dimensional units, the three-dimensional equivalent can be computed with formula 10 in the Supplementary data. (**D**) Mathematical estimation of a Ca^{2+} microdomain near an open ORAI channel (red curve), and around 25 (blue curve) and 50 (black curve) ORAI channels. Single channel current was assumed to be 3.8 fA (Prakriya and Lewis, 2002, 2006; Prakriya *et al*, 2006). EGTA concentration was 1.2 mM, thus, the mean path length (λ) value was ~400 nm. For channel clusters (~60–100 nm wide; Park *et al*, 2009), which are small relative to λ, the clusters can be approximated by a single channel with the sum of all individual channels (Naraghi and Neher, 1997; Neher, 1998). Note that physiological activation of ORAI channels only occurs through the formation of channel clusters directly beneath STIM1 puncta. (**E**, **F**) Cartoons illustrate the physiological (IS) and non-physiological (No IS) activation of T cells. Following IS formation, mitochondria are quickly transported by the actin cytoskeleton (not shown for simplicity) to the IS in the immediate vicinity of ORAI channel clusters (~200 nm away). This translocation allows them to prevent the slow Ca^{2+}-dependent ORAI channel inactivation by reducing the magnitude and/or extension of Ca^{2+} microdomains and thereby sustaining the activity of ORAI channels. In addition, PMCA re-distribute into areas of the PM where mitochondria are present, which induces a significant reduction of local Ca^{2+} microdomain-dependent modulation of PMCA activity. The subcellular organelle distribution induces higher $[Ca^{2+}]_i$, which is translated into more sustained NFAT activity, more efficient T-cell activation and increased cell proliferation. In the absence of IS formation (i.e. TG stimulation), mitochondria do not approach subplasmalemmal areas (<200 nm) and PMCA are not re-distributed in the PM. Therefore, Ca^{2+} microdomains and subsequent subplasmalemmal Ca^{2+} signals are higher, which in turn induce the slow Ca^{2+}-dependent ORAI channel inactivation.

396 nm away from the pore of the channel. Thus, under physiological conditions, the slow Ca^{2+}-dependent inactivation of ORAI channels is controlled by a Ca^{2+} microdomain whose size ranges between ~140 and 400 nm. This covers the distance range (~150–200 nm) between mitochondria and ORAI channels at the IS. Hence, the positioning of mitochondria relative to ORAI1/3 channels can explain the mitochondrial control of CRAC/ORAI channel activity as previously described (Gilabert and Parekh, 2000; Hoth *et al*, 2000; Gilabert *et al*, 2001; Glitsch *et al*, 2002; Quintana *et al*, 2006). In addition, active ORAI channels form clusters (1600–9000 nm^2) (Park *et al*, 2009) upon TG stimulation and cap-like structures after IS formation (Barr *et al*, 2008), which generate larger and higher Ca^{2+} microdomains than that predicted beneath a single channel (Figure 9D). The latter explains why mitochondrial Ca^{2+} uptake and mitochondrial translocation towards the PM (once they reach the area <900 nm from the PM) upon TG stimulation also control CRAC/ORAI channel activity (Quintana *et al*, 2006), although mitochondria never localize within 200 nm of the PM under these conditions. However, mitochondrial control of ORAI channel activity is less efficient in the absence of IS formation, since sustained global Ca^{2+} signals following TG stimulation are significantly lower than global Ca^{2+} signals in the presence of the IS (Figure 4D). We can, therefore, conclude that the IS enhances the mitochondrial control of ORAI channel activity by facilitating a close localization of mitochondria to ORAI channels, which efficiently inhibits the generation of high local Ca^{2+} microdomains at the IS.

While mitochondrial Ca^{2+} uptake has been proven to be essential for the activity of CRAC/ORAI channels in a large variety of cells (Hoth *et al*, 1997; Montero *et al*, 2000; Bakowski *et al*, 2001; Varadi *et al*, 2004; Muñoz *et al*, 2011; Waldeck-Weiermair *et al*, 2011), in certain other cell types mitochondrial Ca^{2+} homeostasis has been described to be irrelevant for the activity of ORAI channels (Giacomello *et al*, 2010). We confirm that global and local Ca^{2+} signals in HeLa cells are much lower than in T cells following TG stimulation. More intrestingly, the ratio between local and global Ca^{2+} signals is significantly higher in HeLa than in Jurkat T cells. This implies that HeLas cells are not very efficient to purge incoming Ca^{2+} through CRAC/ORAI channels away from the PM, which is in full agreement with the data by Pozzan's group (Giacomello *et al*, 2010). However, mitochondrial Ca^{2+} signal increased following voltage-operated Ca^{2+} entry (VOCE) activation (Giacomello *et al*, 2010). This preference of subplasmalemmal mitochondria to sense Ca^{2+} microdomains generated either by VOCE or by CRAC/ORAI channels seems to be highly cell-type specific. Very recently, Muñoz *et al* (2011) demonstrated that mitochondria in vascular smooth muscles cells take up Ca^{2+} from CRAC/ORAI channels but not from VOCE (Muñoz *et al*, 2011). This allows mitochondria to control the Ca^{2+} influx-dependent proliferation of those cells. In case of T cells the major, if not sole, Ca^{2+} influx pathway is the STIM1–ORAI1-mediated capacitative Ca^{2+} entry (Feske *et al*, 2005, 2006). Since T-cell activation requires sustained Ca^{2+} signals for hours, the control of the slow Ca^{2+}-dependent inactivation of CRAC/ORAI channels is essential. Mitochondria are very powerful intracellular Ca^{2+} buffers (Rizzuto and Pozzan, 2006) and are also highly mobile organelles (Yi *et al*, 2004; Quintana *et al*, 2007; Saotome *et al*, 2008; Schwindling *et al*, 2010). Therefore, it is not surprising that T cells accumulate a large amount of mitochondria beneath the IS where the signalling domain for T-cell activation is established. This is now more striking if we consider the large accumulation of STIM1, ORAI1 and PMCA at the IS.

Both the kinetics and the amount of mitochondrial Ca^{2+} uptake have been reported to increase significantly if mitochondria localize close to Ca^{2+} channels (Rizzuto *et al*, 1998). It was therefore not surprising to observe low and heterogeneous Ca^{2+} signals at the IS. Disruption of mitochondrial accumulation into the immediate vicinity of the IS recovered the high and homogeneous Ca^{2+} microdomains beneath the PM. These data are in contradiction to the findings of Lioudyno *et al* (2008), who reported higher Ca^{2+} signals at the T-cell–target cell interface, which were, however, not measured by TIRF. The $[Ca^{2+}]_i$ gradient reported by the authors may be a direct consequence of mitochondrial Ca^{2+} indicator sequestration, which generates apparent $[Ca^{2+}]_i$ gradients in T lymphocytes following TG stimulation or IS formation (Quintana and Hoth, 2004).

Finally, we demonstrated that the contribution of SERCA to Ca^{2+} microdomains is not important as local Ca^{2+} signals at the IS in the presence or absence of TG following formation of a matured IS were very similar. This highlights mitochondria as the major controlling unit of Ca^{2+} microdomains beneath CRAC/ORAI channels at the IS under physiological conditions. However, mitochondria by itself cannot regulate channel activity since they localize around 200 nm away from channel clusters. The local Ca^{2+} domain is likely to influence the activity of Ca^{2+}-binding proteins such as calmodulin. Calmodulin interacts with and induces fast Ca^{2+}-dependent inactivation of ORAI1 and ORAI3 (Mullins *et al*, 2009; Frischauf *et al*, 2011). Differences in the degree of Ca^{2+}-dependent inactivation have been reported for ORAI1, ORAI2 and ORAI3, with ORAI3 showing the strongest fast inactivation but little slow inactivation (Lis *et al*, 2007). Whether calmodulin also influences the slow mitochondrial-dependent inactivation is not known. Calmodulin has also been reported to bind to the polybasic domain of STIM (Bauer *et al*, 2008), where it may affect association of this domain with the PM and subsequently the Ca^{2+} influx through CRAC/ORAI channels. Recently, a new Ca^{2+}-binding protein, CRACR2A, has been described to participate in the formation and stability of STIM–ORAI1 complex (Srikanth *et al*, 2010). Although we do not yet know the threshold affinity of CRACR2A for Ca^{2+}, one can speculate that mitochondrial-dependent Ca^{2+} microdomains around channels may regulate the function of CRACR2A and subsequently CRAC/ORAI channels. By preventing large accumulation of Ca^{2+} near the sites that govern slow inactivation of ORAI channels, mitochondria also reduce the Ca^{2+} microdomain-dependent modulation of PMCA. In this case, even though mitochondria and PMCA co-localize strongly at the IS, we have not found so far any evidence of organelle–protein interaction (data not shown). Nevertheless, since calmodulin has been described to modulate PMCA activity (Brini *et al*, 2003; Caride *et al*, 2007), one can again speculate that calmodulin-dependent PMCA activity would be highly sensitive to the subplasmalemmal Ca^{2+} signal. Therefore, by controlling local Ca^{2+} signals, mitochondria out compete PMCA, avoiding an inefficient Ca^{2+} recycling at the IS and thereby sustaining a long-lasting Ca^{2+} influx through CRAC/ORAI channels. This

results in an enhanced global Ca^{2+} signals and an enlarged NFAT activity (Figure 9E). In contrast, if mitochondria are further away from the PM as is the case in the absence of an IS, local Ca^{2+} microdomains are larger, which subsequently induces slow Ca^{2+}-dependent ORAI channel inactivation, increased PMCA activity, smaller global Ca^{2+} signals and a less efficient NFAT activity (Figure 9F). By specifically arranging mitochondria, ORAI channels and PMCA, the IS thus ensures efficient Ca^{2+}-dependent activation and clonal expansion of T_h cells during the immune response.

Materials and methods

Cells

Human Jurkat T-cell lines were grown as described previously (Quintana and Hoth, 2004). Jurkat F6 cell line was kindly provided by Professor CT Baldari (University of Sienna, Italy). Human peripheral blood lymphocytes and $CD4^+$ T cells were isolated and cultured as previously described (Schwarz *et al*, 2007). To avoid pre-stimulation, $CD4^+$ cells were negatively purified with 'Dynabeads Untouched Human CD4 T Cells' isolation kit from Invitrogen/Dynal following the manufacturer's instructions. The Burkitt's lymphoma B-cell line Raji was obtained from DSMZ (http://www.dsmz.de/) and was grown in RPMI-1640 medium (Invitrogen 21875-034) supplemented with 10% fetal calf serum and 1% of Pen/Strep antibiotic solution (Invitrogen 15140-122). HeLa cells were obtained from DSMZ and cultured in DMEM supplemented with 10% fetal calf serum and 1% Pen/Strep antibiotic solution.

Generation of stable ORAI1-expressing Jurkat T cell lines

Jurkat T cells (clone E6-1) were modified to stably express human ORAI1 with an extracellular HA-tag located between transmembrane segments 3 and 4 (ORAI1–HA) (Feske *et al*, 2006). To that end, the ORAI1–HA ORF was introduced into plasmid HDV (kindly provided by Dr Derya Unutmaz, NYU School of Medicine, USA) *en bloc* with a downstream puromycin selection cassette, by subcloning a continuous fragment from ORAI1–HA-containing vector MO91 (kindly provided by Dr Masatsugu Oh-hora, Department of Cell Signaling, Tokyo Medical and Dental University, Tokyo, Japan). For virus production, the resulting plasmid was co-transfected with pseudotyping plasmid VSV-G into HEK293T cells, employing the calcium phosphate transfection technique. Jurkat T cells were transduced with virus-containing HEK293T cell supernatant and grown in the presence of 3 μg/ml puromycin to enrich for transgene-expressing cells. Finally, clonal populations of ORAI1–HA-expressing Jurkat T cells were obtained using flow cytometric single cell sorting. Homogeneous ORAI1–HA expression after extended culture periods was verified by staining with anti-HA antibody and flow cytometric analysis.

Reagents and antibodies

All chemicals not specifically mentioned were from Sigma (highest grade). Other reagents used in our experiments include fura-2/AM (stock 1 mM in DMSO), Fluo-4FF (stock 10 mM in DMSO), Fluo-5F (stock 1 mM in DMSO), MitoTracker® Green FM (stock 200 μM in DMSO), MitoTracker® DeepRed/AM (stock 200 μM in DMSO), latrunculin B (stock 1 mg/ml in DMSO), latrunculin A (stock 1 mg/ml in DMSO), TG (stock 1 mM in DMSO) from Molecular Probes, anti-human CD3 and anti-human CD28 monoclonal antibodies (mAbs) from Biozol, azid-free activating monoclonal anti-LFA-1 (clone MEM-83) from Acris, anti-ORAI1 (Catalogie number 08264) from Sigma-Aldrich, anti-PMCA (clone 5F10) from Acris. Anti-human CD3 for stimulation with beads was obtained from Diaclone (clone B-B11) and for labelling from Biolegend (clone UCHT-1, coupled with Alexa647). Recombinant staphylococcal enterotoxin E (SEE) was from Toxin Technologies (Sarasota, Florida). Anti-human CD28 mAb for stimulation was obtained from Biozol. Dynabeads®CD3 beads for the cell-cycle experiments were from Invitrogen Dynal AS.

Cloning

hORAI1 or hORAI3 containing an mEGFP-tag at the N- or C-terminus were obtained by inserting PCR-amplified hORAI1 (NM 032790) or hORAI3 (NM 152288) either with or without a termination signal into modified pMax vectors (Lonza) containing either an mEGFP lacking the termination signal followed by an EcoRV site or containing mEGFP with an N-terminal EcoRV site and a C-terminal termination signal, respectively. Alternatively, a pMax vector containing the red fluorescent protein TagRFP-T was used to clone a C-terminally tagged hORAI1 construct. hSTIM1 containing a TagRFP-T tag at the C-terminus was obtained similar to ORAI constructs. All constructs were confirmed by DNA sequencing. The Lifeact-mRFPruby construct was kindly supplied by Dr Ronald Wedlich-Soldner, Max-Planck Institute for Biochemistry, Martinsried, Germany. The EGFP–PMCA4b construct was kindly supplied by Dr Stanley A Thayer from Department of Pharmacology, University of Minnesota Medical School, USA (Pottorf *et al*, 2006).

4D live-cell imaging

Jurka T cells were transfected 48 h before imaging with 5 μg ORAI–mEGFP vector plus 5 μg Lifeact-mRFPruby vector, 2.5 μg ORAI–mEGFP vector plus 5 μg STIM1–TagRFP-T vector or 2.5 μg EGFP–PMCA4b vector using Lonza nucleofection with protocol C-16. To label CD3, the cells were incubated with anti-CD3 Alexa647 antibody (clone UCHT-1) for 30 min at room temperature. Raji cells were incubated for 30 min at room temperature with 10 μg/ml SEE and 2 μM fura-2 to identify them. The cells were resuspended in standard 1 mM Ca^{2+} Ringer's solution (see Ca^{2+} imaging). After settling the Jurkat T cells on poly-L-ornithine-coated coverslips, Raji cells or stimulatory beads (see Ca^{2+} imaging) were added to the Jurkat T cells. The cells were imaged at 37°C using a Zeiss Cell Observer HS widefield microscope equipped with a ×40 Fluar oil lense (N.A. 1.3), a LED fluorescence lamp (Colibri, Zeiss), an objective piezo stepper (PIFOC, PI) and a standard monochrome CCD camera (AxioCam MRm, Zeiss) at binning 2 × 2. Filters were a quadband pinkel set (Semrock), a dualband pinkel set (56HE, Zeiss) and a single-band GFP filter (38HE, Zeiss). A *Z*-volume of 22 μm was imaged at 0.5 μm slice-distance every minute. The acquired images were corrected for crosstalk (Axiovision, Zeiss) and deconvolved by maximum-likelihood estimation algorithm (Huygens, SVI) with measured point spread function (PsSpeck-Kit, Invitrogen). For visualization, *Z*-stacks were projected as maximum intensity projections in XY.

Laser-scanning microscopy of fixed cells

Jurkat T cells and the low-expressing ORAI1-cellline clone J1.14 were fixed with 4% ice-cold paraformaldehyde, permeabilized with PBS/0.5 % Triton-X and stained with anti-ORAI1 or anti-PMCA (Borke *et al*, 1989; Magyar *et al*, 2002) or anti-SERCA 1, 2, 3 (clone H-300, Santa Cruz) primary antibodies as indicated followed by matching secondary antibodies conjugated with Alexa568 (Invitrogen). Images were acquired with a Zeiss LSM 710 equipped with a ×63 LCI Plan-Neofluar glycerine objective with Nyquist criterions matched and deconvolved (except PMCA stainings) by maximum-likelihood estimation algorithm (Huygens, SVI) with measured point spread function (PsSpeck-Kit, Invitrogen). For visualization, *Z*-stacks were projected as maximum intensity projections in XY.

Bioluminescence imaging of NFAT activity in single living cells

Jurkat T cells stably expressing the luciferase reporter gene under control of a triplet of NFAT response elements were cultured in bottom-glass Petri dishes in RPMI-1640 medium containing 10% FCS and 1 mM luciferin. Then Petri dish containing cells was placed in an incubator (Zeiss CTI-controller 3700) with controlled temperature (37°C), CO_2 (5%) and humidity attached over the stage of an inverted microscope (Zeiss Axiovert S100 TV) for photon counting imaging of reporter gene that reflects NFAT transcription factor activity. Then cells were stimulated with TG, anti-CD3 mAbs or anti-CD3 antibody-coated beads. Finally, photonic emissions were captured concurrently with brightfield images with a Hamamatsu VIM photon counting camera handled with an Argus-20 image processor at 15 min intervals for either 6 or 14 h. Transcription activity is expressed as total photonic emissions in each image minus background photonic emissions (specific photonic emissions), as previously reported (Valero *et al*, 2008).

Ca^{2+} imaging

Ca^{2+} imaging and fluorescence measurements MitoTracker® Green FM (Molecular Probes) were carried out as previously described

(Quintana and Hoth, 2004; Quintana *et al*, 2006, 2007) only that ratio images were recorded at intervals of 5 s. Standard 1 mM Ca^{2+} Ringer's solution contained (in mM): 155 NaCl, 4.5 KCl, 1 $CaCl_2$, 2 $MgCl_2$, 10 D-glucose, and 5 Hepes (pH 7.4 with NaOH). $CaCl_2$ was substituted by 1 mM EGTA to prepare 0 Ca^{2+} Ringer's solution or increased to prepare 20 mM Ca^{2+} Ringer's solution. TG (1 μM) alone or together with anti-human CD3 or anti-human CD3/anti-human CD28 antibody-coated beads were used to stimulate Jurkat T cells and $CD4^+$ T cells, respectively. Antibody-coated bead preparation was carried out exactly as described previously (Quintana *et al*, 2007).

Mitochondrial Ca^{2+} measurements

Mitochondrial Ca^{2+} signals were measured and analysed exactly as previously described (Quintana *et al*, 2007, 2009).

Evanescent-wave imaging

TIRFM was carried out as described previously (Quintana *et al*, 2007, 2009). Cells were loaded at 22–23°C for 30–45 min with 10 μM Fluo-4FF/AM, 1 μM Fluo-5F/AM and/or 100–200 nM MitoTracker® Green/AM or 50–100 nM MitoTracker® DeepRed/AM in culture medium containing 10 mM HEPES, washed with fresh medium, stored at RT for 10 min, and immediately used.

In vitro calibration of Fluo-5F

To distinguish the difference between the local and global calcium signal, Ringer solutions with either 0 (1 mM EGTA) or 1 mM Ca^{2+} were supplemented with different concentrations of Fluo-5F pentapotassium salt (1, 5, 7.5, 10, 25, 50, 100 μM) and measured in TIRF and epifluorescence mode under the same conditions as the cells were imaged. We confirmed linear increase of the dye's fluorescence ($R^2 > 0.98$) and calculated the slope a for TIRF and EPI in 0 (1 mM EGTA) and 1 mM Ca^{2+} Ringer solution. R_{min} was estimated as the fluorescence value when the cells were fully depleted of Ca^{2+} (after 0 Ca^{2+}/EGTA/TG treatment for 10 min). This was done for every single cell separately, making it independent from the cell-specific loading of the non-ratiometric dye. R_{max} could then be calculated by taking the ratio of the slopes between 0 (1 mM EGTA) and 1 mM Ca^{2+} Ringer solutions (a_{1Ca}/a_{0Ca}) times R_{min}. The K_d of Fluo-5F is 2.3 μM. The Ca^{2+} concentration was then calculated with the formula:

$$[Ca^{2+}] = (R - R_{min})/(R_{min} \times (a_{1Ca}/a_{0Ca}) - R) \times K_d$$

Electrophysiology

Patch-clamp experiments were performed and analysed as previously described (Fanger *et al*, 1995; Quintana *et al*, 2007). The actin cytoskeleton-disrupting drugs cytochalasin D (10 μM), latrunculin A (10 μg/ml) or latrunculin B (10 μg/ml) were added to the external solution and cells were pre-incubated with the respective drugs for 30, 10 or 10 min, respectively, before recording.

Cell synchronization and cell-cycle analysis

Jurkat T cells were grown in standard RPMI-1640 to a density of $0.8–1.2 \times 10^6$ cells/ml. Cells were synchronized and arrested at different phases of cell cycle. For the initial synchronization of cells at the G_0/G_1 phase, cells were cultured for 48 h in isoleucine-free RPMI-1640 (Invitrus, Switzerland). To arrest the cells at G_1/S border, cells were treated with 200 ng/ml aphidicolin (Sigma) for 24 h in standard culture medium. Cells were thereafter released in standard culture medium for 4 h to enrich the cells at the S phase, followed by treatment with 100 ng/ml nocodazole for 16 h to arrest the cells at the G_2/M phase. Transitions between different culture media were preceded by washing the cells once with PBS. At each time point, T-cells were fixed and stained with DAPI for DNA analysis and used for Ca^{2+}-imaging experiments and high-resolution epifluorescence microscopy in parallel. For DNA analysis, DAPI fluorescence pictures were acquired on a Zeiss Cell Observer with a ×5 objective. Images were automatically segmented with Zeiss Axiovision software and ROIs of cell conglomerates were excluded manually. The densitometric sum of each single ROI was found to best reflect the DNA content. Histograms of single cell values were fitted with the sum of two Gaussian distribution (for G_1 and G_2 phase) and a broadened Gaussian (the product of two sigmoid functions, for S phase). Fitting was performed with Igor Pro 6.0.3.1 (Wavemetrics, Lake Oswego, Oregon), with initial manual guessing and constraints (the broadened Gaussian had to be located between 1.1 and 1.9).

Data analysis

Data were analysed using TILL Vision (TILL Photonics), Igor Pro (Wavemetrics), ImageJ (NIH), AxioVision (Zeiss), Pulse (HEKA), Fit Master (HEKA) and Microsoft Excel (Microsoft). All values are given as mean ± s.e.m. (number of cells). Between three and six independent experiments were performed for each experimental condition. In case, data points were normally distributed, an unpaired two-sided Student's *t*-test was used. If normal distribution could not be confirmed, a non-parametric test (Mann–Whitney) was carried out. *P*-values are stated in the figure legends. Level of significance is indicated in Figures 1, 2 and 6 ($*P<0.05$, $**P<0.01$, $***P<0.001$). For co-localization analysis, we used the ImageJ macro JACoP. The CV of the pixel-to-pixel fluorescence (as a normalized measure of spatial heterogeneity) was defined as the ratio of standard deviation of the raw fluorescence intensity to the mean fluorescence (after subtraction of background signal) over all pixels of the footprint area (Luccardini *et al*, 2009).

Supplementary data

Supplementary data are available at *The EMBO Journal* Online (http://www.embojournal.org).

Acknowledgements

Research carried out for this study with human material has been approved by the local ethics committee. We thank Bettina Strauß and Anja Ludes for excellent technical support. We thank Dr Stanley A Thayer for supplying the EGFP–PMCA4b construct. This project was funded by the Deutsche Forschungsgemeinschaft: SFB 530, project A3, SFB 894, project A1, Graduate College 'Molecular, physiological and pharmacological analysis of cellular membrane transport', and Grant KR 3430/1-1 (with Karsten Kruse) to MH; SFB 894, project A2, Graduate College 'Calcium signalling and nanodomains' to BAN; SFB 530, project C12 to UB) and a competitive intrafaculty Grant from HOMFOR (to AQ).

Author contributions: AQ wrote the MS, did and designed the experiments and analysed the data; MP, CJ, DA-A, HR, CK and LN did and designed the experiments and analysed the data; CV and BAN designed the experiments and analysed the data; PM did the experiments; UB designed the experiments; JR analysed the data; MH wrote the MS, analysed the data and also designed experiments; HR also wrote part of the MS.

Conflict of interest

The authors declare that they have no conflict of interest.

References

Abarca-Rojano E, Muñiz-Hernández S, Moreno-Altamirano MM, Mondragón-Flores R, Enriquez-Rincón F, Sánchez-García FJ (2009) Re-organization of mitochondria at the NK cell immune synapse. *Immunol Lett* **122:** 18–25

Baixauli F, Martín-Cófreces NB, Morlino G, Carrasco YR, Calabia-Linares C, Veiga E, Serrador JM, Sánchez-Madrid F (2011) The mitochondrial fission factor dynamic-related protein 1 modulates T-cell receptor signalling at the immunological synapse. *EMBO J* **30:** 1238–1250

Bakowski D, Glitsch MD, Parekh AB (2001) An examination of the secretion-like coupling model for the activation of the Ca2 + release-activated Ca2 + current I(CRAC) in RBL-1 cells. *J Physiol* **532:** 55–71

Barr VA, Bernot KM, Srikanth S, Gwack Y, Balagopalan L, Regan CK, Helman DJ, Sommers CL, Oh-Hora M, Rao A, Samelson LE (2008) Dynamic movement of the calcium sensor STIM1 and the calcium channel Orai1 in activated T-cells: puncta and distal caps. *Mol Biol Cell* **19:** 2802–2817

Bauer MC, O'Connell D, Cahill DJ, Linse S (2008) Calmodulin binding to the polybasic C-termini of STIM proteins involved in store-operated calcium entry. *Biochemistry* **47:** 6089–6091

Baughman JM, Perocchi F, Girgis HS, Plovanich M, Belcher-Timme CA, Sancak Y, Bao XR, Strittmatter L, Goldberger O, Bogorad RL, Koteliansky V, Mootha VK (2011) Integrative genomics identifies MUC as an essential component of the mitochondrial calcium uniporter. *Nature* (e-pub ahead of print)

Bautista DM, Lewis RS (2004) Modulation of plasma membrane calcium-ATPase activity by local calcium microdomains near CRAC channels in human T cells. *J Physiol* **556:** 805–817

Bautista DM, Hoth M, Lewis RS (2002) Enhancement of calcium signalling dynamics and stability by delayed modulation of the plasma-membrane calcium-ATPase in human T cells. *J Physiol* **541:** 877–894

Borke JL, Caride A, Verma AK, Penniston JT, Kumar R (1989) Plasma membrane calcium pump and 28-kDa calcium binding protein in cells of rat kidney distal tubules. *Am J Physiol* **257:** 842–849

Brini M, Coletto L, Pierobon N, Kraev N, Guerini D, Carafoli E (2003) A comparative functional analysis of plasma membrane Ca2+ pump isoforms in intact cells. *J Biol Chem* **278:** 24500–24508

Cannell MB, Cheng H, Lederer WJ (1995) The control of calcium release in heart muscle. *Science* **268:** 1045–1049

Caride AJ, Filoteo AG, Penniston JT, Strehler EE (2007) The plasma membrane Ca2+ pump isoform 4a differs from isoform 4b in the mechanism of calmodulin binding and activation kinetics: implications for Ca2+ signaling. *J Biol Chem* **282:** 25640–25648

Contento LR, Campello S, Trovato AE, Magrini E, Anselmi F, Viola A (2010) Adhesion shapes T cells for prompt and sustained T-cell receptor signalling. *EMBO J* **29:** 4035–4047

De Stefani D, Raffaello A, Teardo E, Szabo I, Rizzuto R (2011) A forty-kilodalton protein of the inner membrane is the mitochondrial calcium uniporter. *Nature* (e-pub ahead of print)

Dolmetsch RE, Pajvani U, Fife K, Spotts JM, Greenberg ME (2001) Signaling to the nucleus by an L-type calcium channel-calmodulin complex through the MAP kinase pathway. *Science* **294:** 333–339

Dustin ML, Cooper JA (2000) The immunological synapse and the actin cytoskeleton: molecular hardware for T cell signaling. *Nat Immunol* **1:** 23–29

Dustin ML (2005) A dynamic view of the immunological synapse. *Semin Immunol* **17:** 400–410

Dustin ML (2008) T-cell activation through immunological synapses and kinapses. *Immunol Rev* **221:** 77–89

Fanger CM, Hoth M, Crabtree GR, Lewis RS (1995) Characterization of T cell mutants with defects in capacitative calcium entry: genetic evidence for the physiological roles of CRAC channels. *J Cell Biol* **131:** 655–667

Feske S (2007) Calcium signalling in lymphocyte activation and disease. *Nat Rev Immunol* **7:** 690–702

Feske S, Prakriya M, Rao A, Lewis RS (2005) A severe defect in CRAC Ca2+ channel activation and altered K+ channel gating in T cells from immunodeficient patients. *J Exp Med* **202:** 651–662

Feske S, Gwack Y, Prakriya M, Srikanth S, Puppel SH, Tanasa B, Hogan PG, Lewis RS, Daly M, Rao A (2006) A mutation in Orai1 causes immune deficiency by abrogating CRAC channel function. *Nature* **441:** 179–185

Frischauf I, Schindl R, Bergsmann J, Derler I, Fahrner M, Muik M, Fritsch R, Lackner B, Groschner K, Romanin C (2011) Cooperativeness of Orai cytosolic domains tunes subtype-specific gating. *J Biol Chem* **286:** 8577–8584

Giacomello M, Drago I, Bortolozzi M, Scorzeto M, Gianelle A, Pizzo P, Pozzan T (2010) Ca2+ hot spots on the mitochondrial surface are generated by Ca2+ mobilization from stores, but not by activation of store-operated Ca2+ channels. *Mol Cell* **38:** 280–290

Gilabert JA, Parekh AB (2000) Respiring mitochondria determine the pattern of activation and inactivation of the store-operated Ca(2+) current I(CRAC). *EMBO J* **19:** 6401–6407

Gilabert JA, Bakowski D, Parekh AB (2001) Energized mitochondria increase the dynamic range over which inositol 1,4,5-trisphosphate activates store-operated calcium influx. *EMBO J* **20:** 2672–2679

Glitsch MD, Bakowski D, Parekh AB (2002) Store-operated Ca2+ entry depends on mitochondrial Ca2+ uptake. *EMBO J* **21:** 6744–6754

Hoth M, Fanger CM, Lewis RS (1997) Mitochondrial regulation of store-operated calcium signaling in T lymphocytes. *J Cell Biol* **137:** 633–648

Hoth M, Button DC, Lewis RS (2000) Mitochondrial control of calcium-channel gating: a mechanism for sustained signaling and transcriptional activation in T lymphocytes. *Proc Natl Acad Sci USA* **97:** 10607–10612

Kar P, Nelson C, Parekh AB (2011) Selective activation of the transcription factor NFAT1 by calcium microdomains near Ca2+ release-activated Ca2+ channels. *J Biol Chem* **286:** 14795–14803

Korzeniowski MK, Szanda G, Balla T, Spat A (2009) Store-operated Ca(2+) influx and subplasmalemmal mitochondria. *Cell Calcium* **46:** 49–55

Kupfer A, Dennert G, Singer SJ (1983) Polarization of the Golgi apparatus and the microtubule-organizing center within cloned natural killer cells bound to their targets. *Proc Natl Acad Sci USA* **80:** 7224–7228

Kupfer A, Singer SJ (1989) Cell biology of cytotoxic and helper T cell functions: immunofluorescence microscopic studies of single cells and cell couples. *Ann Rev Immunol* **7:** 309–337

Lewis RS (2007) The molecular choreography of a store-operated calcium channel. *Nature* **446:** 284–287

Lioudyno MI, Kozak JA, Penna A, Safrina O, Zhang SL, Sen D, Roos J, Stauderman KA, Cahalan MD (2008) Orai1 and STIM1 move to the immunological synapse and are up-regulated during T cell activation. *Proc Natl Acad Sci USA* **105:** 2011–2016

Lis A, Peinelt C, Beck A, Parvez S, Monteilh-Zoller M, Fleig A, Penner R (2007) CRACM1, CRACM2, and CRACM3 are store-operated Ca2+ channels with distinct functional properties. *Curr Biol* **17:** 794–800

Llinas R, Sugimori M, Silver RB (1992a) Microdomains of high calcium concentration in a presynaptic terminal. *Science* **256:** 677–679

Llinas R, Sugimori M, Silver RB (1992b) Presynaptic calcium concentration microdomains and transmitter release. *J Physiol Paris* **86:** 135–138

Luccardini C, Yakovlev AV, Pasche M, Gaillard S, Li D, Rousseau F, Ly R, Becherer U, Mallet JM, Feltz A, Oheim M (2009) Measuring mitochondrial and cytoplasmic Ca2+ in EGFP expressing cells with a low-affinity calcium Ruby and its dextran conjugate. *Cell Calcium* **45:** 275–283

Magyar CE, White KE, Rojas R, Apocada G, Friedman PA (2002) Plasma membrane Ca2+-ATPase and NCX1 Na+/Ca2+ exchanger expression in distal convoluted tubule cells. *Am J Physiol Renal Physiol* **283:** 29–40

Montero M, Alonso MT, Carnicero E, Cuchillo-Ibáñez I, Albillos A, García AG, García-Sancho J, Alvarez J (2000) Chromaffin-cell stimulation triggers fast millimolar mitochondrial Ca2+ transients that modulate secretion. *Nat Cell Biol* **2:** 57–61

Mueller P, Quintana A, Griesemer D, Hoth M, Pieters J (2007) Disruption of the cortical actin cytoskeleton does not affect store operated Ca^{2+} channels in human T-cells. *FEBS Lett* **581:** 3557–3562

Mullins FM, Park CY, Dolmetsch RE, Lewis RS (2009) STIM1 and calmodulin interact with Orai1 to induce Ca2+ dependent inactivation of CRAC channels. *Proc Natl Acad Sci USA* **106:** 15495–15500

Muñoz E, Valero RA, Quintana A, Hoth M, Núñez L, Villalobos C (2011) NSAIDs inhibit vascular smooth muscle cell proliferation by enabling the Ca^{2+} dependent inactivation of CRAC/Orai channels normally prevented by mitochondria. *J Biol Chem* **286:** 16186–16196

Naraghi M, Neher E (1997) Linearized buffered Ca2+ diffusion in microdomains and its implications for calculation of [Ca2+] at the mouth of a calcium channel. *J Neurosci* **17:** 6961–6973

Neher E (1998) Vesicle pools and Ca2+ microdomains: new tools for understanding their roles in neurotransmitter release. *Neuron* **20:** 389–399

Oh-hora M, Rao A (2008) Calcium signaling in lymphocytes. *Curr Opin Immunol* **20:** 250–258

Park CY, Hoover PJ, Mullins FM, Bachhawat P, Covington ED, Raunser S, Walz T, Garcia KC, Dolmetsch RE, Lewis RS (2009) STIM1 clusters and activates CRAC channels via direct binding of a cytosolic domain to Orai1. *Cell* **136:** 876–890

Pottorf II WJ, Johanns TM, Derrington SM, Strehler EE, Enyedi A, Thayer SA (2006) Glutamate-induced protease-mediated loss of plasma membrane Ca2+ pump activity in rat hippocampal neurons. *J Neurochem* **98:** 1646–1656

Prakriya M, Solaro CR, Lingle CJ (1996) [Ca2 +]i elevations detected by BK channels during Ca2 + influx and muscarine-mediated release of Ca2 + from intracellular stores in rat chromaffin cells. *J Neurosci* **16:** 4344–4359

Prakriya M, Lewis RS (2002) Separation and characterization of currents through store-operated CRAC channels and Mg2 + -inhibited cation (MIC) channels. *J Gen Physiol* **119:** 487–507

Prakriya M, Lewis RS (2006) Regulation of CRAC channel activity by recruitment of silent channels to a high open-probability gating mode. *J Gen Physiol* **128:** 373–386

Prakriya M, Feske S, Gwack Y, Srikanth S, Rao A, Hogan PG (2006) Orai1 is an essential pore subunit of the CRAC channel. *Nature* **443:** 230–233

Quintana A, Hoth M (2004) Apparent cytosolic calcium gradients in T-lymphocytes due to fura-2 accumulation in mitochondria. *Cell Calcium* **36:** 99–109

Quintana A, Kummerow C, Junker C, Becherer U, Hoth M (2009) Morphological changes of T cells following formation of the immunological synapse modulate intracellular calcium signals. *Cell Calcium* **45:** 109–122

Quintana A, Schwarz EC, Schwindling C, Lipp P, Kaestner L, Hoth M (2006) Sustained activity of CRAC channels requires translocation of mitochondria to the plasma membrane. *J Biol Chem* **281:** 40302–40309

Quintana A, Schwindling C, Wenning AS, Becherer U, Rettig J, Schwarz EC, Hoth M (2007) T cell activation requires mitochondrial translocation to the immunological synapse. *Proc Natl Acad Sci USA* **104:** 14418–14423

Rizzuto R, Pozzan T (2006) Microdomains of intracellular Ca2 + : molecular determinants and functional consequences. *Physiol Rev* **86:** 369–408

Rizzuto R, Pinton P, Carrington W, Fay FS, Fogarty KE, Lifshitz LM, Tuft RA, Pozzan T (1998) Close contacts with the endoplasmic reticulum as determinants of mitochondrial Ca2 + responses. *Science* **280:** 1763–1766

Roberts WM (1993) Spatial calcium buffering in saccular hair cells. *Nature* **363:** 74–76

Sanchez-Madrid F, del Pozo MA (1999) Leukocyte polarization in cell migration and immune interactions. *EMBO J* **18:** 501–511

Saotome M, Safiulina D, Szabadkai G, Das S, Fransson A, Aspenstrom P, Rizzuto R, Hajnóczky G (2008) Bidirectional Ca2 + -dependent control of mitochondrial dynamics by the Miro GTPase. *Proc Natl Acad Sci USA* **105:** 20728–20733

Schwarz EC, Kummerow C, Wenning AS, Wagner K, Sappok A, Waggershauser K, Griesemer D, Strauss B, Wolfs MJ, Quintana A, Hoth M (2007) Calcium dependence of T cell proliferation following focal stimulation. *Eur J Immunol* **37:** 2723–2733

Schwindling C, Quintana A, Krause E, Hoth M (2010) Mitochondria positioning controls local calcium influx in T cells. *J Immunol* **184:** 184–190

Spitzer NC (2006) Electrical activity in early neuronal development. *Nature* **444:** 707–712

Srikanth S, Jung HJ, Kim KD, Souda P, Whitelegge J, Gwack Y (2010) A novel EF-hand protein, CRACR2A, is a cytosolic Ca^{2+} sensor that stabilizes CRAC channels in T cells. *Nat Cell Biol* **12:** 436–446

Valero RA, Senovilla L, Nunez L, Villalobos C (2008) The role of mitochondrial potential in control of calcium signals involved in cell proliferation. *Cell Calcium* **44:** 259–269

Varadi A, Cirulli V, Rutter GA (2004) Mitochondrial localization as a determinant of capacitative Ca2 + entry in HeLa cells. *Cell Calcium* **36:** 499–508

Waldeck-Weiermair M, Jean-Quartier C, Rost R, Khan MJ, Vishnu N, Bondarenko AI, Imamura H, Malli R, Graier WF (2011) The leucine zipper EF hand-containing transmembrane protein 1 (LETM1) and uncoupling proteins-2 and 3 (UCP2/3) contribute to two distinct mitochondrial Ca2 + uptake pathways. *J Biol Chem* (e-pub ahead of print)

Yi M, Weaver D, Hajnoczky G (2004) Control of mitochondrial motility and distribution by the calcium signal: a homeostatic circuit. *J Cell Biol* **167:** 661–672

Yog R, Barhoumi R, McMurray ND, Chapkin SR (2010) n-3 Polyunsaturated fatty acids suppress mitochondrial translocation to the immunologic synapse and modulate calcium signaling in T cells. *J Immunol* **184:** 5865–5873

